JGP Journal of General Physiology

VIEWPOINT

Structure versus function: Are new conformations of pannexin 1 yet to be resolved?

Carsten Mim[1], Guy Perkins[2], and Gerhard Dahl[3]

Pannexin 1 (Panx1) plays a decisive role in multiple physiological and pathological settings, including oxygen delivery to tissues, mucociliary clearance in airways, sepsis, neuropathic pain, and epilepsy. It is widely accepted that Panx1 exerts its role in the context of purinergic signaling by providing a transmembrane pathway for ATP. However, under certain conditions, Panx1 can also act as a highly selective membrane channel for chloride ions without ATP permeability. A recent flurry of publications has provided structural information about the Panx1 channel. However, while these structures are consistent with a chloride selective channel, none show a conformation with strong support for the ATP release function of Panx1. In this Viewpoint, we critically assess the existing evidence for the function and structure of the Panx1 channel and conclude that the structure corresponding to the ATP permeation pathway is yet to be determined. We also list a set of additional topics needing attention and propose ways to attain the large-pore, ATP-permeable conformation of the Panx1 channel.

Introduction

Initially, the pannexin field got off to an inauspicious start. Because the three proteins of the pannexin family (Panx1, Panx2, and Panx3) were discovered on the basis of their limited sequence homology to the invertebrate innexin gap junction proteins, it was assumed that they, too, would form gap junctions (Panchin et al., 2000; Bruzzone et al., 2003). However, notwithstanding some disputed science, it soon became clear that the gap junction function of pannexins is not realized (Dahl and Locovei, 2006; Huang et al., 2007; Sosinsky et al., 2011). Gap junction formation by pannexins is moreover prevented by glycosylation of the Panx1 protein (Boassa et al., 2007; Penuela et al., 2007; Boassa et al., 2008). It is conceivable, however, that the nonglycosylated form of Panx1 could allow the docking of oligomers in apposing membranes to each other. Indeed, such docking was observed in cryo-EM preparations of a mutant Panx1, N255A (Ruan et al., 2020). However, because glycosylation of the protein is required for membrane trafficking (Boassa et al., 2007; Penuela et al., 2007), it is unlikely that this process occurs in vivo. This notion is supported by the observation that a glycosylation mutant of Panx1 failed to lead to junctional conductance between paired oocytes, while expression of wtPanx1 followed by glycosidase F treatment before pairing of the cells resulted in gap junction formation, albeit at a much reduced rate as compared with the rate observed with connexins (Boassa et al., 2008). Furthermore, the gap junction function also is unlikely because of theoretical reasons and experimental findings, including expression in single cells, such as erythrocytes (Locovei et al., 2006a), and exclusive expression in the apical membrane of polarized epithelial cells (Ransford et al., 2009; Hanner et al., 2012; Shum et al., 2019). Of the three pannexins, only Panx1 has been studied in detail, and a clear channel function is well established for it. Therefore, this Viewpoint will exclusively deal with Panx1.

It is generally assumed that an important function of Panx1 is to form ATP release channels. For example, as of this writing, a PubMed search with "pannexin" and "ATP release" as search terms yielded 287 publications. However, the biophysical evidence for this function is sparse, and the supporting evidence is largely correlative and/or based on pharmacological or genetic interference with ATP release. The ATP release function of Panx1 channels has been contested based on evidence that the channels are highly selective for Cl^- and the lack of detectable ATP release under the experimental conditions, i.e., activation by voltage, used in these studies (Ma et al., 2012; Romanov et al., 2012).

It was long held that the oligomeric state of the Panx1 channel is that of a hexamer (Penuela et al., 2013; Dahl, 2015; Chiu et al., 2018). Recently, in a <6-mo period, six research groups independently published similar cryo-EM structures of the Panx1 membrane channel (Deng et al., 2020; Jin et al., 2020; Michalski et al., 2020; Mou et al., 2020; Qu et al., 2020; Ruan et al., 2020).

[1]Department of Biomedical Engineering and Health Systems Royal Institute of Technology, Huddinge, Sweden; [2]National Center for Microscopy and Imaging Research, University of California, San Diego School of Medicine, La Jolla, CA; [3]Department of Physiology, University of Miami School of Medicine, Miami, FL.

Correspondence to Gerhard Dahl: gdahl@miami.edu.

All these papers challenge the view of the oligomeric state of the channel. Instead of the hexameric arrangement of identical Panx1 subunits, the channel appears to be formed by a homomeric heptamer.

It is uncontested that the Panx1 channel can operate in a conformation in which the channel exhibits a unitary conductance of <100 pS. However, it has also been reported that, under certain experimental conditions, the channel can exhibit several subconductances with very rare sojourns to a maximal conductance of ∼500 pS (Dahl 2015).

Activation of the Panx1 channel can be obtained by various stimuli, some physiological or pathological, others in the form of experimental tools. The majority of the physiological stimuli involve ligands, including ATP, glutamate, α adrenergic agonists, and bradykinin, binding to their cognitive receptors and leading to opening of Panx1 channels and "secondary" ATP release (Dahl 2015, 2018). A nonreversible activation of the channel is induced by cleavage with caspase 3 or 8 (Chekeni et al., 2010), leading to cell death. Experimental stimulation can be obtained in some cells but not in others by increasing the extracellular K^+ concentration (Silverman et al., 2009; Wang and Dahl 2018; Chiu et al., 2018).

Here, we present a point of view on these contested issues in the Panx1 field and attempt to reconcile apparently contradictory data or their interpretations. In addition, we ask to what extent the new structural data support the functional data.

The structure of Panx1 channels as revealed by cryo-EM

The excitement for the long-awaited Panx1 structure was rewarded with not one but six publications, all appearing within the first half of 2020 and using cryo-EM to image the channel (Deng et al., 2020; Jin et al., 2020; Michalski et al., 2020; Mou et al., 2020; Qu et al., 2020; Ruan et al., 2020). Five of the six Panx1 publications showed human Panx1 structures (Deng et al., 2020; Jin et al., 2020; Michalski et al., 2020; Mou et al., 2020; Qu et al., 2020; Ruan et al., 2020), and two showed frog Panx1 structures (Deng et al., 2020; Michalski et al., 2020). To stabilize the frog Panx1 structure, thus improving the resolution for cryo-EM, Michalski et al. (2020) truncated the C terminus by 71 amino acids and removed 24 amino acids from the intracellular loop between transmembrane (TM) helices 2 and 3; this truncation was the version reported. The other publications reported full-length Panx1 structures, although one used a truncated Panx1 variant (Ruan et al., 2020) and another used a mutation (Jin et al., 2020) as their principal references. Because the C terminus–truncated structure and the (combined) WT structure had the highest overall quality of the several Panx1 structures presented by Ruan et al. (2020), it was used for de novo model building, as the reference structure for analyses, and for discussion. For the same reason, Jin et al. (2020) used the double mutation D376E/D379E, which eliminated the caspase-cleavage site, for their de novo model building. The overall architecture and dimensions of the human and frog Panx1 structures were similar, and the extracellular domains (ECDs) and transmembrane domains (TMDs) were nearly identical, except that the N-terminal helix (NTH) of the frog Panx1 is positioned on the intracellular side and not within the TMD as reported in human Panx1. These structures are becoming an important and critical tool to guide functional experiments and open a new venue to perform molecular dynamics simulations.

The most novel finding shared by all the Panx1 structures is that instead of the hexamer hitherto believed to represent the native state of the Panx1 channel, the cryo-EM data show unequivocally a homo-heptamer arranged around a central symmetry axis that constitutes the principal permeation pathway. Panx1's structural envelope adopts an inverted pail shape in the view parallel to the membrane. The heptameric channel is ∼110 Å long and ∼100 Å wide, with a flat ECD protruding ∼35 Å above the cell membrane and an intracellular domain (ICD) extending ∼35 Å into the cytoplasm with the TMD in between (Fig. 1). Both the N and C termini reside on the cytoplasmic side of the channel. Each TMD has four membrane-spanning helices per protomer. The TMD pore is predominantly lined by hydrophobic amino acids. The NTH is short and lines the TMD pore (human Panx1) with the NTH of one subunit interacting with the TMD of the adjacent subunit. Thus, it has been proposed that the NTH helps to maintain a rigid TMD pore (Ruan et al., 2020). Both the extracellular and intracellular pore entrances are lined with positively charged amino acids, making them favorable for negatively charged cargos such as Cl^- and ATP to enter and leave the pore.

A cap structure is formed on the extracellular side from seven ECDs, one from each subunit. The ECDs are organized into the pore's most constricted site, thus defining the maximum size of permeable molecules and establishing the extracellular entrance to the TMD. Each ECD contains one helix cross-linked through a disulfide bond to a three-stranded antiparallel β-sheet. The N-terminal end of each subunit helix protrudes inward toward the central pore axis contributing to the constriction site. The key residues involved in the gating of Panx1 are part of the W74-R75-D81 inter-subunit triplet (Fig. 1) from the N-terminal ends of the ECD helices and are proposed to provide rigidity to the extracellular entrance containing positive charges (Deng et al., 2020). This ring lining the wall of the constriction defines a hydrated pore diameter of ∼9 Å (Fig. 1) and is the crux of the argument that the extracellular constriction site is the effective selectivity filter discriminating cargoes on the basis of their charge and size. By contrast, the narrowest point of the pore in the TMD has a hydrated diameter of ∼13 Å.

Other inter-subunit interactions that stabilize the pore arrangement in the TMD are (1) the F67-Y79 aromatic–aromatic and Q266-T252 hydrogen bonding in the ECD, (2) the TM helix TM1-TM1 and TM2-TM4 interfaces between adjacent subunits, (3) the N-terminal loop from the neighboring subunit extending into the TMD pore lining, and (4) the resolvable residues of C-terminal helix 3 association with the cytoplasmic linker helices 1 and 2 from the adjacent subunit (Fig. 1; Deng et al., 2020; Michalski et al., 2020). In addition, membrane lipids occupy the crevice between TM3 and an adjacent TM4 at the edge of the channel. Lipid head groups associate with positively charged residues from the N-terminal end of TM3 (K214) and the C-terminal domain of TM4 (R302 and K303; Deng et al., 2020). It may be that the lipid environment influences the assembly and possibly the activation of the Panx1 channel.

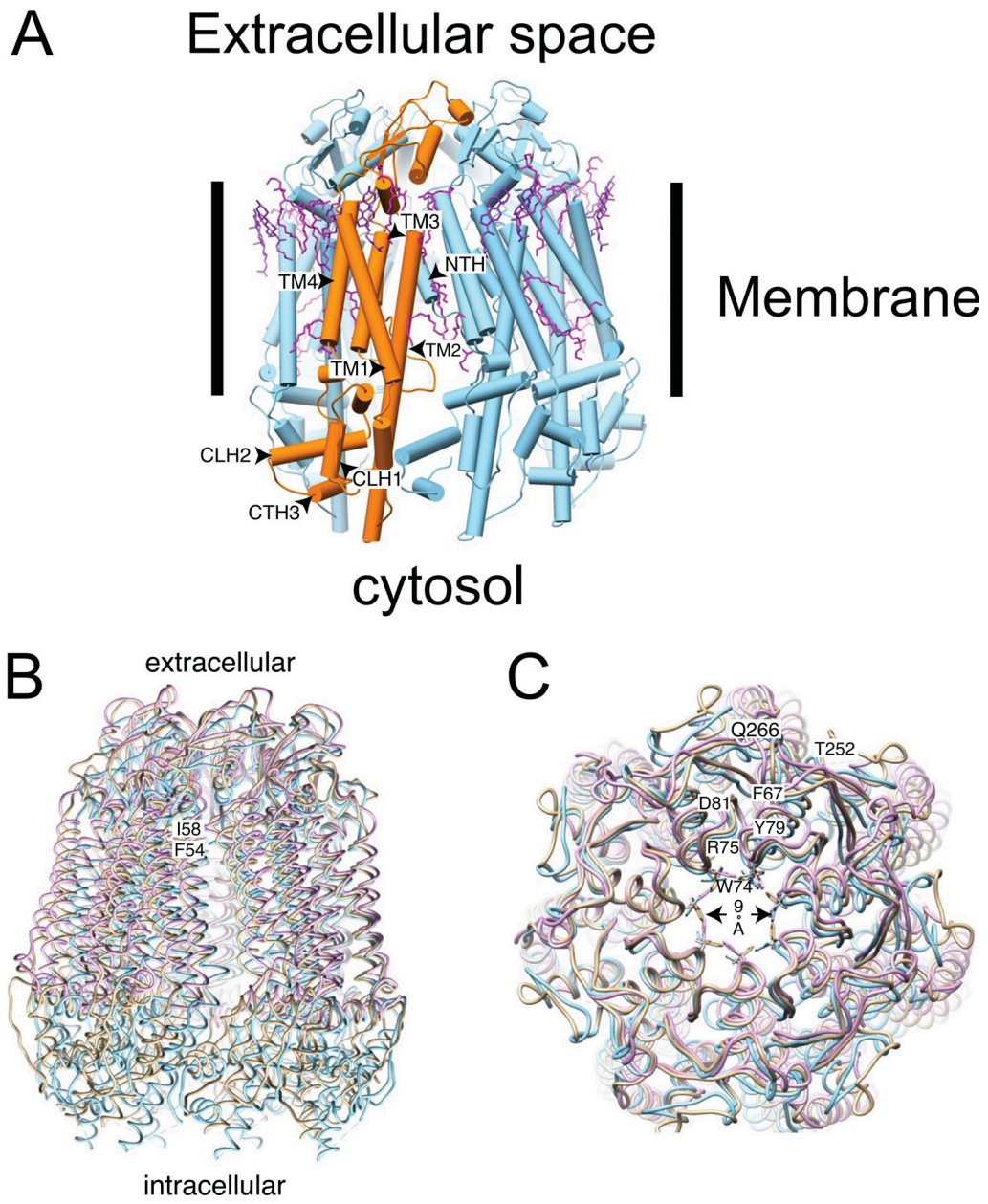

Figure 1. **Structural model of Panx1. (A)** Cartoon representation of Panx1 WT (PDB accession no. 6wbk) stabilized with detergent. The approximate position of the membrane is indicated by the bars. One protomer of the heptameric assembly is indicated in orange. The lipids resolved in the structure are colored in magenta. It is notable that many of the resolved lipids are found at the interface between subunits. CTH, C-terminal helix; CLH, cytoplasmic linker helix. **(B)** Overlay of different Panx1 cryo-EM–based structures from different groups (PDB accession no. 6lto = gold, WT hPanx1; PDB accession no. 6wbk = blue, hPanx1 ΔC terminus, ΔN terminus; PDB accession no. 6v6d = lilac, WT hPanx1). The structures diverge very little in the ECD and the membrane domain. However, the variation is larger in the ICD. The approximate positions of F54 and I58 are indicated. **(C)** Comparison of the extracellular pore. Key residues are annotated using their one-letter abbreviation. All structures are shown as backbone traces except W74, which is part of the constriction ring of the pore. The narrowest constriction is indicated by the arrow.

The pore substantially widens toward the intracellular side. The ICDs extend away from the pore axis, producing a voluminous intracellular vestibule. Two helices in the ICD connect to two TMD helices to form a compact assembly that provides rigidity to the vestibule. The vestibule is slightly larger in the frog Panx1 structure, but the pore architecture is essentially the same as in the human version. The C-terminal segment consisting of ∼70 amino acids, including the caspase cleavage site located immediately before the C terminus, was not visualized in any of the published cryo-EM structures, suggesting that it is intrinsically flexible. C-terminal cleavage removes its autoinhibitory effect without inducing an overall conformational change to the pore (Jin et al., 2020).

A novel feature presented by Ruan et al. (2020) is seven narrow side tunnels in the upper ICD running perpendicular to and ending at the pore, like a T-intersection. This tunnel

network was proposed to allow passage of small anions because each tunnel contains several positively charged and other polar residues along its length. The flexible NTH-TM1 linker would function as a gate. They hypothesized that these side tunnels facilitate Cl^- flux when the pore is blocked by the C terminus residing in the ICD vestibule. Movement or cleavage of the C terminus then would induce the ATP-permeable large-pore conformation. Further structural work is needed to determine whether the C terminus actually resides in the ICD vestibule. One complication with this tunnel hypothesis is that each tunnel has two constriction sites formed by R29 and A33, with diameters of 5.8 and 4.0 Å, respectively, meaning that partial dehydration of a Cl^- ion is likely required for it to pass through the tunnel. The possibility of anion tunnels in the Panx1 structure raises the question: could there be multiple open (active) conformations, and does "open" mean open to ATP and Cl^- ion or Cl^- ion only? Three of the six papers (Michalski et al., 2020; Qu et al., 2020) assume that the Panx1 structure is in the closed or inactive conformation, whereas the other three report an open or active conformation. These discrepancies should be resolved with further work. Interestingly, the overlay of three of these structures, one presumably open and two closed, shows nearly identical conformations of the extracellular constriction of the pore (Fig. 1 C).

The structures of Panx1 truncation and mutant variants, as well as its docked inhibitor, carbenoxolone (CBX), illuminate the roles of distinct structural elements. For example, cryo-EM revealed that CBX sits atop the ECD and plugs the W74-R75-D81 ring (Jin et al., 2020; Ruan et al., 2020), supporting pore blocking as its mechanism of Panx1 inhibition. Second, removal of the NTH did not much change the shape of the TMD. This truncation still generated a CBX-sensitive, voltage-dependent current similar to the full-length Panx1 current (Ruan et al., 2020), suggesting that the NTH may play a role in the assembly of the heptamer from the Panx1 protomers rather than being an essential element in the pore conduction pathway. Third, the Panx1 structures obtained in the presence of Ca^{2+} and K^+ were indistinguishable from the untreated Panx1 structure, suggesting that neither Ca^{2+} nor K^+ is likely to directly activate the Panx1 channel (Ruan et al., 2020). Fourth, the glycosylation-deficient mutant (N255A) generated gap junction structures as well as hemichannels as determined by cryo-EM (Ruan et al., 2020). The N255A gap junction is formed by two hemichannels docked by the interaction of the extracellular linker 2 on apposing ECDs. Ruan et al. (2020) noted that this Panx1 gap junction likely is not a normal physiological conformation.

Comparing the Panx1 structure with other ATP-permeant pore structures offers a blueprint for dissecting pore properties of Panx1. The oligomeric configuration of the ATP-permeant channels does not appear to correlate with pore diameter, in particular when comparing the narrowest extent of the pore (Table 1). Like Panx1, CALHM1 was originally thought to adopt a hexameric configuration (Siebert et al., 2013) until the cryo-EM structure revealed an octameric configuration (Syrjanen et al., 2020). It should be noted that not all connexin channels transport ATP. For example, Cx26, Cx30, Cx43, and Cx46 transport ATP, but Cx32 does not (Harris, 2001; Hansen et al., 2014). An interesting comparison can be made between Panx1 and human Cx31.3. Cx31.3 has a pore with a constriction site diameter of ∼8 Å, similar to Panx1's constriction of ∼9 Å, and also selectively transports Cl^- and ATP (Lee et al., 2020). One difference between the two structures is that the constriction is in the ICD's NTH for Cx31.3 and in the ECD for Panx1. Lee et al. (2020) pointed out that because Cx31.3's pore constriction at the cytoplasmic entrance is smaller than the effective hydrated diameter of ATP (∼12 Å; Sabirov and Okada, 2004), the reported conformation would not allow ATP to pass through the pore without substantial conformational changes of the NTH. The same argument could be applied to Panx1's ECD.

In a comparison of structural motifs, Panx1's protomer shares a motif of four TMD helices with connexins, innexins, CALHM1 and 2, and volume-regulated anion channel (VRAC) protomers. They also share ECD topological similarities, but differences are manifested as well. For example, Panx1 and innexin6 have their ECD2 nestled between the inner and outer lobes of ECD1. CALHM1 and 2 and VRAC do not, and the outer lobe of ECD1 is absent in Cx46 (Myers et al., 2018; Deng et al., 2020; Flores et al., 2020; Qu et al., 2020). In Panx1 and VRAC, residues in the ECD1 helix form the pore constriction site, whereas in Cx46 and innexin6, the NTH forms the constriction in the middle of the TMD. Also, Panx1, innexin6, and CALHM2 have two ECD disulfide bonds, whereas Cx46 has three. The NTH of Panx1 is unique among ATP-permeant channels because it resides in the TMD pore close to the ECD, whereas the NTH in connexins and innexins is in the TMD closer to the ICD (Maeda et al., 2009; Myers et al., 2018; Flores et al., 2020), and the NTH in VRAC is in the ICD near the membrane face (Deneka et al., 2018; Kasuya et al., 2018; Kefauver et al., 2018). In Panx1, connexins, innexins, and VRAC, TM1–TM4 are arranged anticlockwise as viewed from intracellular side, with TM1 nestled between TM2 and TM4, but the CALHM2 arrangement is clockwise and TM1 is attached to TM3. Finally, even though the ICD helix 1 is long, it is not involved in inter-subunit interactions, whereas in CALHM2, the equivalent cytoplasmic helix 1 is nearly parallel to the membrane and forms extensive inter-subunit interactions (Choi et al., 2019; Syrjanen et al., 2020).

Biophysical properties and function of Panx1 channels

While the Panx1 structures obtained in six different laboratories are remarkably congruent, including the structures from different species, this is not the case for several functional aspects. It is now generally accepted that, contrary to original beliefs, pannexins do not form gap junctions despite their classification as "gap junction proteins" (Sosinsky et al., 2011). Instead, Panx1 is well documented to form a plasma membrane channel, which allows the exchange of solutes between the cytoplasm and the extracellular space.

The first demonstration of Panx1 channel function involved the activation of the channel by positive membrane potentials in excess of +20 mV (Bruzzone et al., 2003). Robust Panx1-mediated membrane currents induced by positive membrane voltage were subsequently reported by various laboratories (Pelegrin and Surprenant, 2006; Iglesias et al., 2008; Iglesias et al., 2009b; Qiu and Dahl, 2009; Bunse et al., 2009;

Table 1. **Comparison of oligomeric configuration with pore constriction diameter**

ATP-permeant channel	Oligomeric configuration	Pore constriction diameter (Å)	Reference
VDAC	Monomer (β barrel)	25	Colombini, 2012
Cx26	Hexamer	14 (open), 6 (closed)	Maeda et al., 2009; Nielsen et al., 2012
Cx31.3	Hexamer	8 (closed?)	Lee et al., 2020
Cx43	Hexamer	25 (open), 18 (closed)	Nielsen et al., 2012
Cx46	Hexamer	14	Myers et al., 2018; Flores et al., 2020
VRAC	Hexamer	12–14 (open), 2–5 (closed)	Deneka et al., 2018; Kasuya et al., 2018; Kefauver et al., 2018; Osei-Owusu et al., 2018
Panx1	Heptamer	9	Deng et al., 2020; Jin et al., 2020; Michalski et al., 2020; Mou et al., 2020; Qu et al., 2020; Ruan et al., 2020
Innexin6	Octamer	18	Oshima et al., 2016
CALHM1	Octamer	19.5	Syrjanen et al., 2020
CALHM2	Undecamer	50 (open), 23 (inhibited)	Choi et al., 2019
CALHM4	Decamer, undecamer	20 (without current), 30 (without current)	Drożdżyk et al., 2020

Prochnow et al., 2009; Silverman et al., 2009; Bunse et al., 2011; Gründken et al., 2011; Ma et al., 2012; Romanov et al., 2012; Zhan et al., 2012; Nomura et al., 2017). In oocytes expressing rodent Panx1, the currents are in the microampere range, and in these as in mammalian cells, the currents exhibit strong outward rectification.

Weak Panx1 channel activation by positive membrane voltage was described, which could be boosted substantially by the insertion of a glycine-serine motif immediately after the first methionine (Michalski et al., 2018). Human and mouse Panx1 behaved similarly in these experiments, while mammalian cell lines (HEK and CHO) yielded different current densities for both pannexins. Frog Panx1 was subsequently found to exhibit similar voltage-sensitive properties (Michalski et al., 2020). In contrast, complete absence of voltage activation has been reported for human and frog Panx1, while mouse Panx1 was found to be weakly voltage sensitive (Chekeni et al., 2010; Chiu et al., 2018; Narahari et al., 2021).

The first physiological role ascribed to Panx1 was that of a permeation pathway for ATP, allowing the efflux of ATP to act as an external signal to cells via activation of purinergic receptors (Bao et al., 2004). Subsequently, hundreds of publications affirmed the ATP release functions of Panx1 in multiple cell types based mainly on pharmacological and/or genetic interference. However, the role of Panx1 as an ATP-release channel has been challenged by data obtained with biophysical measurements. It has been shown that the voltage-activated Panx1 channel was highly selective for chloride ions and did not exhibit detectable ATP release (Ma et al., 2012; Romanov et al., 2012; Wang et al., 2014). On the other hand, several groups reported ATP release and/or activation of Panx1 currents after exposure of cells to high extracellular potassium ion (K^+) concentrations (Silverman et al., 2009; Santiago et al., 2011; Heinrich et al., 2012; Suadicani et al., 2012; Michalski and Kawate, 2016; Qu et al., 2020). However, a lack of K^+-mediated activation of Panx1 has also been reported (Chiu et al., 2018; Nielsen et al., 2020).

Neither high positive membrane potentials nor high extracellular K^+ concentrations can be considered physiological stimuli. A third stimulus for Panx1 activity, cleavage of C-terminal amino acids by caspase, occurs exclusively in apoptotic cells (Chekeni et al., 2010). A correlation of caspase cleavage with ATP release has been established (Chekeni et al., 2010; Boyd-Tressler et al., 2014; Imamura et al., 2020). However, whether caspase cleavage of Panx1 per se causes ATP release remains to be determined. The similarity of the electrophysiological profiles of the voltage-activated and the caspase-cleaved Panx1 channels (Chiu et al., 2017; Wang and Dahl, 2018) raises the question whether caspase by itself is sufficient for initiating ATP release.

However, if we accept that physiological ATP release mediated by Panx1 occurs in a reversible fashion, as proposed in >200 publications, there must be an as-yet-unidentified gating mechanisms, since the activation mechanisms presently documented are either irreversible or unphysiological. Erythrocytes, for example, release ATP reversibly in a low oxygen environment but also in response to shear stress (Locovei et al., 2006a; Sridharan et al., 2010; Forsyth et al., 2011; Cinar et al., 2015; Zhang et al., 2018), two unrelated stimuli converging on the same ATP release channel Panx1.

While it appears that the Panx1 field is riddled with controversies, the following paragraphs show that this is not necessarily so. It can safely be assumed that most, if not all, published data are correct. It may take only a little tuning of the interpretations to get a more coherent picture of the Panx1 field.

Evidence for ATP release mediated by Panx1 channels

Based on the biophysical properties of the channel formed by Panx1, its function as an ATP release channel was proposed soon after its discovery (Bao et al., 2004; Dahl and Locovei, 2006; Locovei et al., 2006a). Ever since, supporting evidence has been accumulated by a large number of researchers, as documented in

several reviews (Dahl and Locovei, 2006; Scemes et al., 2007; MacVicar and Thompson, 2010; Sosinsky et al., 2011; Penuela et al., 2013; Dahl, 2015). Key evidence includes the localization of Panx1 expression matching the site of ATP release at the apical membrane of polarized epithelial cells such as in the airways or renal tubules (Ransford et al., 2009; Hanner et al., 2012). Interestingly, in polarized cells releasing ATP at the basolateral membrane, this function is exerted by another release channel, CALHM (Taruno et al., 2013; Kashio et al., 2019). Additional evidence for the involvement of Panx1 in ATP release is that knockout of Panx1 expression attenuates ATP release (Iglesias et al., 2009a; Qiu et al., 2011; Qu et al., 2011; Suadicani et al., 2012). Furthermore, mutations of Panx1 and chemical modification of the protein affect ATP release (Wang and Dahl, 2010; Qiu et al., 2012).

Evidence that Panx1 channels can be Cl^- selective and lack ATP permeability

The ATP release function has been challenged, however, also based surprisingly on sound biophysical evidence (Ma et al., 2012; Romanov et al., 2012; Wang et al., 2014; Wang and Dahl, 2018). No ATP release was observed in voltage-clamped, Panx1-expressing HEK cells over the voltage range of −50 to +80 mV, despite robust CBX-sensitive currents at positive potentials (Romanov et al., 2012). Similarly, oocytes expressing Panx1 did not release ATP when the membrane potential was clamped at −60, 0, or +40 mV. However, CBX-sensitive ATP release was observed at the same holding potentials in the presence of high extracellular K^+ concentrations (Fig. 2 A; Wang et al., 2014). Instead, the exclusively voltage-activated Panx1 channel was found to be highly selective for Cl^-. Substitution of extracellular Cl^- by larger anions resulted in attenuation of the membrane currents and a large shift of the reversal potential from negative to positive membrane potentials in both HEK cells and *Xenopus laevis* oocytes (Fig. 3, A, B, and D; Ma et al., 2012; Romanov et al., 2012; Chiu et al., 2014; Nomura et al., 2017; Li et al., 2018; Wang and Dahl, 2018). Thus, the Panx1 channel is highly selective for Cl^- and lacks ATP permeability under the experimental conditions used in the referenced studies. Furthermore, in measuring the permeability of the Panx1 channel, it was found that substitution of extracellular Na^+ by larger cations changed neither the reversal potential nor the amplitude of the currents in response to voltage steps or voltage ramps, indicating lack of cation permeability (Ma et al., 2012; Wang et al., 2018; Michalski et al., 2020).

Lack of cation permeability, however, appears to be restricted to the voltage-activated Panx1 channel. The only direct measure of ATP permeability presently available indicates that the ATP-permeable conformation of the Panx1 channel also is permeable to cations (Bao et al., 2004; Locovei et al., 2006a). In an isolated membrane patch subjected to a K^+-ATP gradient, the channel currents reversed neither at the K^+ nor the ATP^{2-} reversal potential, but in between the two (closer to the K^+ equilibrium potential). Furthermore, uptake of positively charged dyes is considered to be an acceptable surrogate for channel-mediated ATP release (Dahl, 2015; Johnson et al., 2016; Chiu et al., 2018). Thus, under conditions of ATP release, the channel does not discriminate on the basis of charge. However, since dye uptake can be mediated by various other mechanisms, including other membrane channels such as gasdermin D (de Vasconcelos et al., 2019) or CALHM (Siebert et al., 2013), dye uptake per se cannot be used as evidence for the involvement of Panx1.

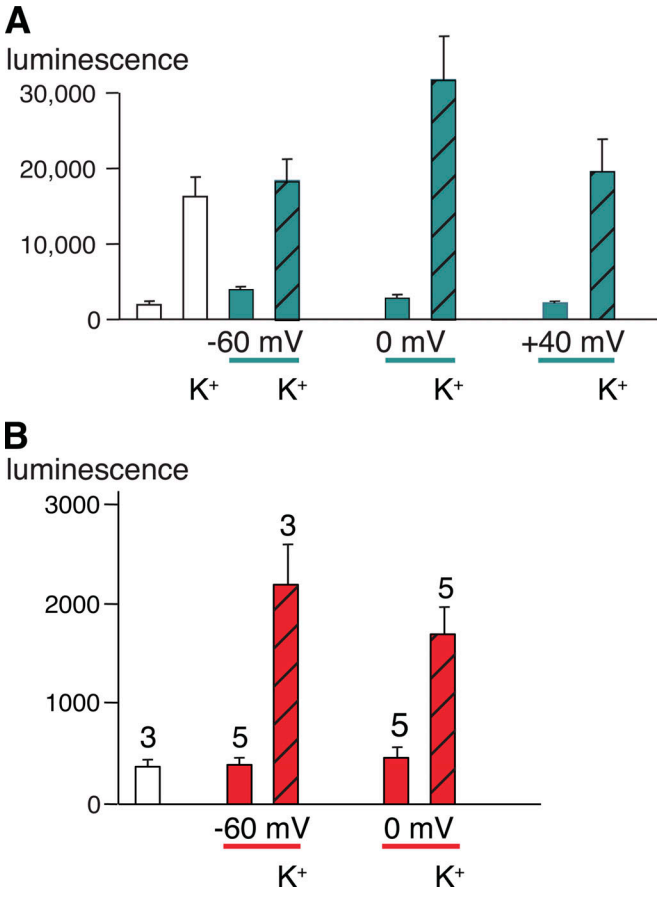

Figure 2. **ATP release by oocytes expressing Panx1. (A)** Oocytes expressing WT Panx1. All colored bars represent data obtained under voltage-clamp conditions; white bars are data from unclamped cells. ATP in the medium was measured as luciferase luminescence. ATP release from Panx1-expressing oocytes induced by potassium gluconate (KGlu) without and with holding the membrane potential under voltage-clamp conditions at −60, 0, or +40 mV, was determined 20 min after initiating the stimulus. Voltage-clamp conditions are indicated with teal lines below the graph and teal bars in the graph. The presence of 150 mM KGlu (K^+ label) is indicated, and the data are displayed as hatched bars. Data are shown as means ± SD; n = 5 for each measurement. Adapted from Wang et al., 2014. **(B)** Oocytes expressing the truncation mutant Panx1Δ378. Oocytes were not voltage clamped (white bar) or were clamped at −60 or 0 mV (red bars). The cells were exposed to oocyte Ringer solution or to a solution containing 85 mM KGlu (K^+ label, hatched bars) as indicated, for 10 min. An aliquot of the supernatant was analyzed for the presence of ATP with the luciferase/luciferin assay. Means ± SE; n as indicated above each bar. Adapted from Wang and Dahl, 2018. Because oocytes expressing Panx1Δ378 have a shortened life span (Jackson et al., 2014), measurements had to be taken in a short time window after injection of mRNA at 80× lower concentration than wtPanx1. Thus, ATP release data cannot be compared between wtPanx1- and Panx1Δ378-expressing cells.

Can Panx1 be both a Cl^--selective and a nonselective channel?

The Panx1 channel was activated by voltage when it was shown to have high selectivity for Cl^- and to lack both cation and ATP

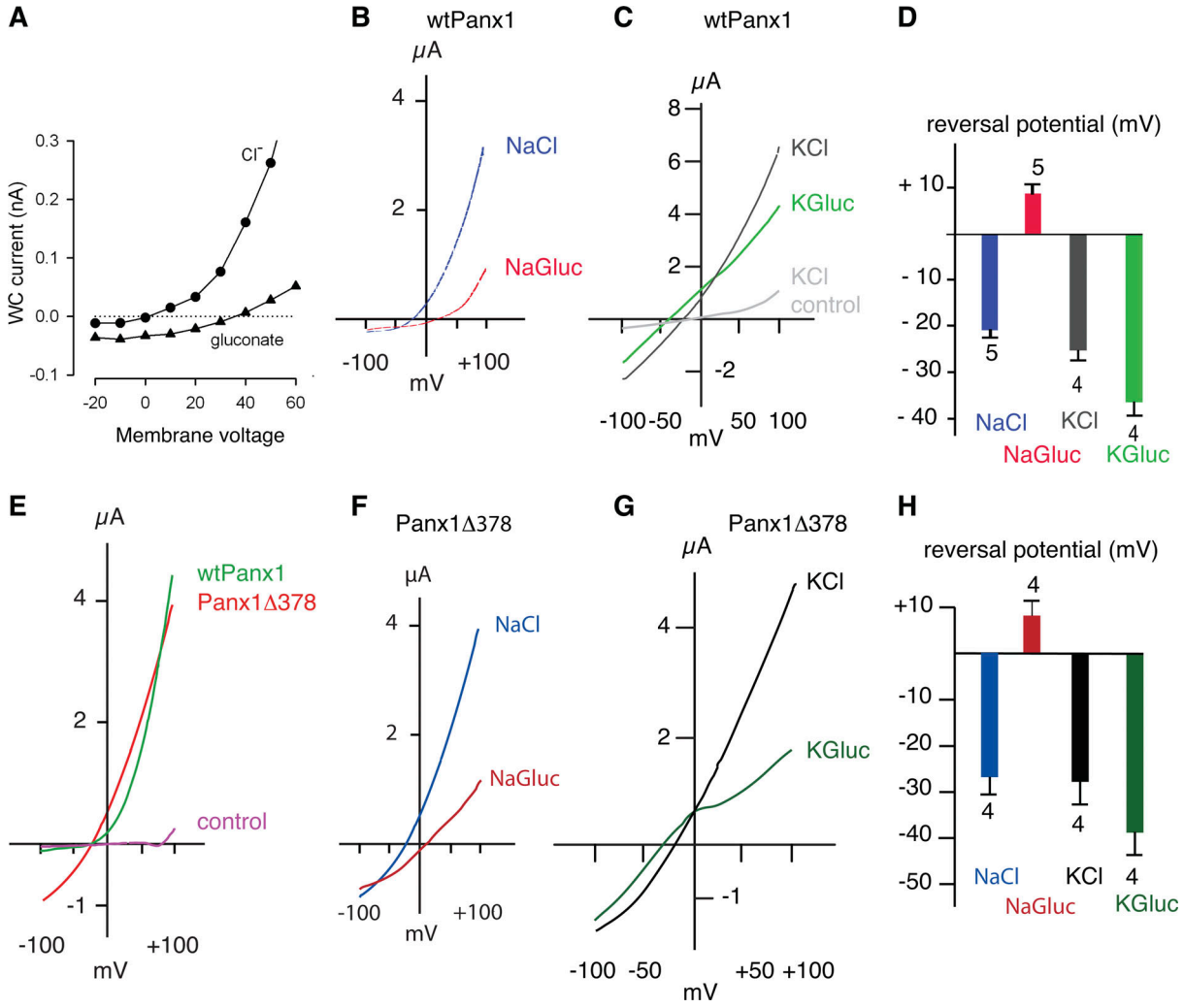

Figure 3. **Current–voltage relations of mouse WT Panx1 and Panx1Δ378. (A)** Replacing extracellular Cl^- by gluconate$^-$ in a voltage step protocol applied to HEK cells expressing Panx1 exogenously attenuated the membrane currents and shifted the reversal potential to a positive potential. Adapted with permission from *Journal of Cell Science* (Romanov et al., 2012). **(B)** Similarly, in oocytes expressing Panx1 exogenously, replacement of Cl^- by gluconate$^-$ (NaGluc) resulted in a shift of the reversal potential to positive values and an attenuation of the currents induced by a voltage ramp from −100 to +100 mV. **(C)** Voltage ramp–induced currents of wtPanx1-expressing oocytes in KCl solution (black trace) were substantially larger than the currents in uninjected control cells under identical conditions (gray trace). Replacing Cl^- by gluconate$^-$ in the bath solution of the same oocyte resulted in attenuation of the currents and a shift of the reversal potential to more negative potential (green trace). **(D)** Quantitative analysis of reversal potentials after anion replacement shows a shift from positive to negative potentials with K^+ as the extracellular cation. Means ± SE; n = 5 (wtPanx1). **(E)** Voltage ramp–induced membrane currents of WT Panx1 channels (green trace) and of channels formed by the truncation mutant Panx1Δ378, where C-terminal amino acids after aspartate 378 are deleted. Uninjected oocytes served as control (magenta trace). Because Panx1Δ378-expressing cells had a short life span, mRNA was injected 80× diluted as compared with WT, and measurements were performed in a 24-h window. Thus, the current amplitudes of WT Panx1 and Panx1Δ378 cannot be compared. In contrast to WT Panx1 channels, those formed by Panx1Δ378 were active over a wide voltage range, yet currents through both types of channels reversed at the same membrane potential. **(F)** Similar to WT Panx1, currents through Panx1Δ378 channels reversed at negative membrane potential with extracellular chloride (blue trace) and at positive potential with gluconate solution (red trace). **(G)** Similar to WT Panx1 channels, replacement of chloride by gluconate ions resulted in the currents reversing at negative potentials when Panx1Δ378-expressing cells were exposed to high extracellular K^+. **(H)** Quantitative analysis of reversal potentials of membrane currents carried by Panx1Δ378 after anion replacement shows a shift from positive to negative potentials with K^+ as the extracellular cation. Means ± SE; n = 4. **(B–H)** Data from Wang and Dahl (2018).

permeability (Romanov et al., 2012; Ma et al., 2012; Wang et al., 2014; Wang and Dahl 2018). This activation was unphysiological, however, for the membrane potential had to be at high positive potentials for Panx1-mediated currents to be detectable. In contrast, all the evidence supporting the ATP release function involved alternative activation mechanisms. Several stimuli, including oxygen deprivation and mechanical stress, trigger channel-mediated ATP release through Panx1 channels (Locovei et al., 2006a; Thompson et al., 2006) This "primary" ATP release is complemented by a "secondary" ATP release (Dahl, 2018), in which a ligand binding to its cognizant receptor opens Panx1 and releases ATP. This process initially explained ATP-induced ATP release (Locovei et al., 2006b) and has now been demonstrated to apply to many other ligands and receptors, including NMDA, angiotensin II, and α adrenergic receptors (Thompson et al., 2008; Billaud et al., 2011; Murali et al., 2014). The function of

secondary ATP release is to boost the cytoplasmic signal, which in all known cases is $[Ca^{2+}]_i$. This amplification is achieved by ATP binding to P2Y receptors, triggering further Ca^{2+} release from intracellular stores.

We propose that the Panx1 channel has at least two distinct open conformations with different permeabilities. When activated by high positive voltage or when truncated at the caspase cleavage site, the channel is highly selective for Cl^- and has no cation or ATP permeability. In contrast, it has been inferred that when opened in physiological settings by various stimuli, the channel is permeant to ATP and allows the TM flux of cationic and anionic dyes. The latter permeability properties can experimentally be induced by high extracellular K^+ concentrations, as verified by changes in the reversal potential and high rate of ATP release. However, since activation by extreme voltage or by K^+ is unphysiological, it seems prudent to reexamine with biophysical measurements the permeability properties of the Panx1 channel when activated physiologically, i.e., by ligand binding to receptors known to activate Panx1.

Activation of Panx1 by extracellular K^+

ATP release in a variety of cell types can be stimulated by raising the extracellular K^+ concentration; based on pharmacological interference, the release has been attributed to Panx1 channels (Bao et al., 2004; Qiu and Dahl, 2009; Silverman et al., 2009; Santiago et al., 2011; Heinrich et al., 2012; Suadicani et al., 2012; Wang et al., 2013). The ATP release shown in one of the published cryo-EM studies also used K^+ to stimulate ATP release (Qu et al., 2020). Since an increase in extracellular K^+ depolarizes the plasma membrane, it is logical to assume that depolarization is the trigger for the release (Heinrich et al., 2012). However, the shift in membrane potential induced by K^+ should not be sufficient to bring the Panx1 channel into the voltage range where it is fully active. Indeed K^+-induced Panx1-mediated currents were observed under voltage-clamp conditions over a wide voltage range (Silverman et al., 2009). The slow time course of the K^+-induced Panx1 activation also speaks against depolarization as the critical step. Substitution of several amino acids in the extracellular loops of Panx1 by alanine modulated the response (Wang et al., 2018). Among the substitutions attenuating the K^+ effect were amino acids W74 and R75, which are part of the external constriction observed in all published cryo-EM structures. Alanine substitution of amino acid D241 in the second extracellular loop resulted in amplification of the K^+ response. Although the alanine substitution effects are suggestive for a direct action of K^+ on Panx1 through binding and/or gating, the very slow activation of Panx1-mediated currents indicates that the mechanism responsible could be more complex. Additional evidence for K^+-activation of Panx1 channels comes from the observation that currents carried by Panx1 were inhibited in a cysteine replacement mutant ($Panx1^{T62C,\ C426S}$) by the thiol reagent 2-(trimethylammonium)ethyl methanethiosulfonate regardless of whether voltage or K^+ served as stimulus (Wang et al., 2014).

It has been shown that unpaired connexons also exhibit sensitivity to extracellular K^+. For example, replacement of extracellular Na^+ with K^+ resulted in a reversible >10-fold potentiation of Cx50 hemichannel currents (Srinivas et al., 2006). As observed for Panx1 channels, the effect of K^+ on Cx50 channels was observed under voltage-clamp conditions, excluding depolarization as a mechanism.

It appears that the K^+-induced activation of Panx1 may not work in all cell types. For example, Panx1 currents were induced in CHO cells by K^+ (Michalski and Kawate, 2016), while HEK cells expressing Panx1 exogenously did not respond to increased extracellular K^+ with an induction of CBX-sensitive currents (Chiu et al., 2018). The discrepancy in cell responses to K^+ could be due to the involvement of additional factors, which could be facilitating in some cell types or inhibitory in others. The observation of a lack of K^+ effect on the cryo-EM structure is consistent with such a scenario (Ruan et al., 2020). However, the solution of this problem could be much more trivial. In the experiments where K^+ failed to activate Panx1 in cells, the extracellular solution contained millimole concentrations of Ca^{2+} (Chiu et al., 2018; Nielsen et al., 2020). Because divalent cations, including Ca^{2+}, interfere with the K^+ effect on Panx1 (Wang et al., 2018), a response would not be expected under these conditions.

Whatever the detailed mechanism of the Panx1 channel activation by K^+ may be, the Cl^- selectivity of the channel is not evident in high extracellular K^+ (Fig. 3, C and D). Replacement of extracellular Cl^- by gluconate resulted in Panx1-mediated currents, which reversed at negative potentials instead of the reversal at positive potentials observed in the absence of the K^+ stimulus. In high extracellular K^+, the Panx1 channels were active over the whole voltage range from −100 to +100 mV, yielding membrane currents with amplitudes exceeding the endogenous oocyte currents by far (see also Fig. 3 C; Silverman et al., 2009; Wang et al., 2018).

ATP release studies under voltage clamp conditions have shown that Panx1 channel activity induced by membrane depolarization does not result in ATP release (Romanov et al., 2012; Wang et al., 2014). However, ATP release was detected when the extracellular solution contained high K^+ concentrations at negative, zero, or positive membrane potentials (Fig. 2 A).

The extracellular $[K^+]$ required to activate Panx1 channels exceeds by far the physiological concentration of the ion. However, like the activation by voltage, the K^+ stimulus is an experimentally convenient tool. More importantly, under pathological conditions, such as epilepsy, stroke, or central nervous system trauma, the extracellular $[K^+]$ can exceed 50 mM (Somjen, 1979; Gidö et al., 1997; Sick et al., 1998), thereby activating Panx1. Moreover, at these concentrations, K^+ interferes with the negative feedback of ATP on Panx1 channel function (Qiu and Dahl, 2009; Qiu et al., 2012; Jackson et al., 2014). Alanine scanning mutagenesis suggests partially overlapping amino acids in the extracellular loops being involved in both activation of Panx1 channels by K^+ and inhibition of the channel by ATP (Qiu et al., 2012; Wang et al., 2018).

Activation of Panx1 by caspase cleavage

A completely different activation for Panx1 channels has been discovered in apoptotic cells and involves the cleavage of 48 (mouse) or 47 (human) C-terminal amino acids by caspase

(Chekeni et al., 2010). Certainly, this is an irreversible process associated with cell death. Nevertheless, this mechanism has found general acceptance as a physiological function of Panx1, despite the fact that in normal cells ATP release is reversible and consequently cannot involve cleavage of the C terminus. Because a deletion mutant mimicking the caspase cleaved Panx1 has no cytoplasmic plug of the sort observed in the WT Panx1 structure, this has been said to provide a structural basis for the cleaved Panx1's ATP permeability (Ruan et al., 2020).

With caspase cleavage, the channel becomes constitutively active, with a high open probability not only at positive potentials, but also at potentials as low as −100 mV (Chekeni et al., 2010; Jackson et al., 2014; Chiu et al., 2017; Chiu et al., 2018; Wang and Dahl, 2018). Fig. 3 E shows the current–voltage relationship of WT Panx1 channels and that of Panx1Δ378, a truncation mutant mimicking the caspase-cleaved Panx1 (Wang and Dahl, 2018). Panx1Δ378 was active over the whole voltage range of −100 to + 100 mV. Thus, caspase cleavage has a profound effect on channel gating by increasing the open probability at negative membrane potentials. In their original report, Chekeni et al. (2010) reported that apoptosis, ATP release, and caspase cleavage of Panx1 were correlated. However, it was not clear whether the anti-Fas stimulus for apoptosis itself caused the large pore conformation, before or while the channel was rendered constitutively active by the cleavage, which sealed the apoptotic fate of the cells.

Subsequent data on the caspase-cleaved Panx1 channel published by the same group raised doubts about the ATP permeability of the truncated channel in the absence of another stimulus. They reported that the cleaved channel has the same selectivity for Cl^- as the exclusively voltage-activated channel (Chiu et al., 2014). The voltage-activated channel, however, has been reported not to be ATP or cation permeable (Ma et al., 2012; Romanov et al., 2012; Wang et al., 2014). Because neither cleavage nor truncation at the caspase site affected the reversal potential (Chiu et al., 2017), it can be expected that the selectivity of the caspase-cleaved channel did not change either compared with the voltage-activated WT Panx1 channel.

The lack of effect on the reversal potential is particularly puzzling in the experiments involving concatemers of the Panx1 protein. The concatemers were designed to allow sequential removal of C-terminal tails in a hexameric channel. As expected, this resulted in a "quantal" activation of the channel, with each cleavage of a protomer leading to an incremental increase in single-channel conductance (Chiu et al., 2017). The data also show a continuous increase in current density in whole-cell recordings as more caspase sites within the concatemer were used. Yet, the ATP release was discontinuous, requiring removal of more than two C termini. Thus, there was selective (Cl^-?) current in the absence of ATP release. However, this change in selectivity was not reflected in the voltage ramps applied to the channels with variable numbers of cleaved C termini; all currents reversed at exactly the same potential. In these experiments, collecting periods of 4 to 8 h were used to determine ATP released into the supernatant, which are orders of magnitude longer than typically used in ATP release studies, attenuating the confidence level for interpretation of the measured values. During this time period, many events of cell division and apoptosis could have been the source of extracellular ATP. In contrast, ATP release by airway epithelial cells was detectable within seconds after a sudden osmotic stimulus, was reversible, and was attenuated by the Panx1 inhibitors CBX or probenecid (Ransford et al., 2009). Similarly, ATP release by Schwann cells induced by hypotonicity was detectable within 2 min after the stimulus, occurred in the absence of the cytoplasmic marker lactate dehydrogenase, and was blocked by the same Panx1 inhibitors (Wei et al., 2021). Furthermore, ATP release by oocytes expressing WT Panx1 or Panx1Δ378 was detectable in the unstirred supernatant as early as 5 min after a K^+ stimulus (Wang and Dahl, 2018). Even in apoptotic cells, ATP release and that of metabolites was observed in a shorter time scale when a complex signaling chain was initiated by anti-Fas or UV treatment (Chekeni et al., 2010; Medina et al., 2020). Intriguingly, different sets of metabolites were released depending on the apoptosis stimulus. UV radiation and anti-Fas stimulation had only a small subset of metabolites, including ATP, in common, while the majority of metabolites released in response to the two stimuli did not overlap (Medina et al., 2020). This observation suggests that different signaling modalities modify the selectivity of the Panx1 channel or that other release mechanisms were involved concurrently.

Both voltage- and caspase-activated channels have different unitary conductances at negative potentials (~15 pS) as compared with positive potentials (~90 pS; Ma et al., 2012; Romanov et al., 2012; Chiu et al., 2017). Since physiological ATP release occurs at the normal or slightly depolarized membrane potential, i.e., at negative potentials, the ~15-pS conformation rather than the ~90-pS channel would need to be responsible for ATP release. Permeability measurements with Panx1 truncated at the caspase cleavage site (Panx1Δ378) and involving extracellular ion replacement confirmed the Cl^- selectivity and lack of cation permeability like the WT Panx1 channel (Fig. 3, F and H; Wang and Dahl, 2018). However, in the presence of extracellular K^+, Cl^- selectivity was attenuated (Fig. 3, G and H), while cation permeability and ATP permeability became apparent just as in WT Panx1 channels (Wang and Dahl, 2018).

As observed for WT Panx1 channels, Panx1Δ378 channels did not release ATP under voltage-clamp conditions despite robust membrane currents (Wang and Dahl, 2018). Extracellular K^+ not only boosted the membrane currents of Panx1Δ378 channels but also induced ATP release with the membrane potential clamped at −60 or 0 mV (Fig. 2 B; Wang and Dahl, 2018).

Recently, data obtained with purified Panx1 protein in lipid bilayers and liposomes were interpreted in support of the view that caspase cleavage is sufficient to induce the ATP-permeable conformation of the Panx1 channel (Narahari et al., 2021). Indeed, the data show properties expected from Panx1 channels in the ATP-permeable conformation, including cation permeability and flux of ATP and of dyes with a preference of anionic over cationic dyes. However, the data also show that the caspase-activated Panx1 channel in lipid bilayers is distinct from the caspase-activated Panx1 channel in mammalian cells. In bilayers, three populations of channels were observed. One group of channels exhibited a single channel conductance of 100 pS,

which is similar to the one observed in mammalian cells. The second group has been shown to dwell mainly in a 189-pS state. The third group did not require caspase cleavage and was observed only transiently after insertion of the protein into the lipid bilayer. The channels in this group exhibited variable conductance states with a maximal conductance of ∼400 pS.

Another distinction of the Panx1 channel in lipid bilayers from the channel in mammalian cells is the lack of rectification. In mammalian cells, the caspase-cleaved Panx1 channel exhibits a 12-pS conductance at negative membrane potentials and a conductance of 96 pS at positive potentials (Chiu et al., 2017). In contrast, in lipid bilayers the voltage–current relationship was linear over a voltage range of −200 to +200 mV (Narahari et al., 2021). Thus, the disposition of the purified and caspase-cleaved Panx1 channel to allow the flux of ATP and other molecules is much more favorable in lipids than in mammalian cells. A channel with a conductance of ∼200 pS at the resting membrane potential or a depolarized potential consistent with physiological events is not the same as the 12-pS channel in mammalian cells. In the lipid bilayer, the channel is not only exposed to a different lipid environment, but it is also missing the protein environment prevailing in intact cells. It will be intriguing to see whether lipids or proteins prevent the transition from the 12-pS to the ∼200-pS channel conformation and how this is regulated in cells. Overall, the data obtained with purified Panx1 in an exclusive lipid environment support the hypothesis of more than one open conformation of the Panx1 channel.

Thus, although caspase cleavage of Panx1 may not be sufficient for ATP release, this process does not interfere with other stimuli for the release. For example, in oocytes expressing Panx1 truncated at the caspase cleavage site, the channel was constitutively active, yielding membrane currents, which were boosted further by extracellular K^+. Furthermore, ATP release via the truncated Panx1 was observed only with the additional K^+ stimulus (Wang and Dahl, 2018). The ATP release observed in apoptotic/pyroptotic cells, therefore, may be the consequence of other stimuli. This release, however, plays a key role in the attraction of macrophages or microglia to injured or sick cells, a process working in vertebrate and invertebrate organisms (Chekeni et al., 2010; Samuels et al., 2010; Samuels et al., 2013). In the invertebrate nervous system, the ATP signal, rather than being a "find me" signal (Chekeni et al., 2010), appears to serve as a mobilization signal for microglial cells (Duan et al., 2009; Dahl and Muller, 2014).

What is the oligomeric state of the Panx1 channel?

Until recently, it was held that Panx1 oligomerizes to form a homomeric hexameric channel (Penuela et al., 2013; Chiu et al., 2018). This conclusion was based on cross-linking studies (Boassa et al., 2007; Chiu et al., 2017; Epp et al., 2019) and EM with negative staining of the isolated protein (Wang et al., 2014; Chiu et al., 2017). Acceptance of these findings was facilitated because a hexameric oligomeric state of Panx1 matched that of connexin "hemichannels" (the half of gap junction channels in one of the two opposing plasma membranes). Cross-linking studies in general suffer from both under- and overestimation of protein interactions. If the cross-linking agent is applied in very low concentrations and/or for an insufficiently long period, native interactions may not be captured fully, and using high concentrations for excessive periods of time can result in fortuitous linkages, resulting in overestimation of the oligomeric state. Interestingly, in one of the cross-linking studies on Panx1 (Epp et al., 2019), monomeric Panx1 predominated, followed by intermediate oligomers (dimers and trimers), while the apparent hexameric form was barely detectable. In this setting, heptamers, even if present, would have escaped detection because of an insufficient amount of protein in that oligomeric state. These observations, although consistent with incomplete cross-linking, also could indicate that the majority of Panx1 molecules are not assembled to a functional channel. Instead, the intermediate oligomers may only acutely form a functional channel upon a still-mysterious stimulus. Given the existence of dimers and trimers, the functional channel may be a hexamer (2 + 2 + 2 or 3 + 3), but also could be a heptamer (2 + 2 + 3) or higher oligomer.

While the visualization of single-particle Panx1 channels by negative stain appears to support the hexameric state of the channel, the imposed sixfold symmetry used in both studies (Wang et al., 2014; Chiu et al., 2017) could have biased the outcome. However, the support for the hexameric arrangement of the Panx1 channel culminated in the use of concatemers of Panx1 forcing the formation of hexamers. Not only were these concatemers shown to form functional channels, but these channels exhibited biophysical properties essentially identical to those of WT Panx1 channels (Chiu et al., 2017). Thus, the channel formed by WT Panx1 ought to have the same oligomeric state as the one formed by the concatemer. It is conceivable that instead of forming the expected hexamer, one protomer of a concatemer would incorporate into the channel to form a heptamer with other concatemers. However, Chiu et al. (2017) emphasized the hexameric state with Western blots and the exact number of quantal steps predicted for a hexamer. However, like Panx1, CALHM1 was originally thought to adopt a hexameric configuration based on concatemers (Siebert et al., 2013) until the cryo-EM structure revealed an octameric configuration (Syrjanen et al., 2020).

The oligomeric state of the Panx1 channel has been challenged in six publications, all appearing within the first half of 2020 and using cryo-EM to image the channel (Deng et al., 2020; Jin et al., 2020; Michalski et al., 2020; Mou et al., 2020; Qu et al., 2020; Ruan et al., 2020). Instead of the hexamer hitherto believed to represent the native state of the Panx1 channel, the cryo-EM data show unequivocally a homo-heptamer forming the Panx1 channel. However, it would be desirable to have the heptameric arrangement be supported by independent methods. So far, the heptameric assembly supports the closed and the small, Cl^--selective conformations of the Panx1 channel, but not the large-pore conformation. It needs to be seen whether the ATP-permeable Panx1 channel has the same heptameric arrangement or whether higher-order oligomers need to form to render the channel ATP permeable.

Do cryo-EM structures support an ATP release function of Panx1?

In the Panx1 structure publications (Deng et al., 2020; Jin et al., 2020; Michalski et al., 2020; Mou et al., 2020; Qu et al., 2020;

Ruan et al., 2020), the reported narrowest width of the pore, or narrowest exclusion width of the closed conformation for the Panx1 structures, is remarkably uniform—8–9.4 Å. It is worth noting that the extracellular constriction has the same dimensions for all the reported structures, irrespective of whether the C or N terminus is cleaved off (Fig. 1 C shows three overlaid structures). For Panx1 to function as an ATP release channel, the pore must be at least the size of an ATP molecule with an effective hydrated diameter of ATP of ∼12 Å (Sabirov and Okada, 2004) and a hydrodynamic diameter of ATP of 15.4 Å (Rostovtseva and Bezrukov, 1998). Indeed, a surface model of ATP is a poor fit in the cryo-EM map (Fig. 4 A). As seen in a side view of the pore, the ATP molecule resides below the external constriction. The diameter of ATP (mol wt 507) exceeds that of the constriction, making a passage unlikely. As shown in Table 1, other ATP release channels exhibit a considerably wider pore. The situation for the tracer molecule Yo-Pro (mol wt 375) appears to be somewhat more favorable (Fig. 4 B). It is conceivable that, despite the tight fit, thermal fluctuations of the pore and the tracer molecule could enable the Yo-Pro molecule to squeeze through the pore at a low rate.

For reference, the minimal pore diameter of other ATP release channels is ≥14 Å (Table 1). The CALHM 1 channel, for example, is an octamer with a pore diameter of 19.5 Å at its narrowest part. Interestingly, CALHM 1 originally also was considered to be a hexamer (Ma et al., 2016), but cryo-EM data show that the channels formed by various CALHM isoforms are all higher-order oligomers, including octamers, decamers, and undecamers (Choi et al., 2019; Drożdżyk et al., 2020; Syrjanen et al., 2020). CALHM 4 even has been shown to exhibit two oligomeric states with different pore diameters of 20 and 30 Å (Drożdżyk et al., 2020).

The heptameric Panx1 channel with an 8–9.4-Å constriction is a poor candidate to represent a channel conformation with high ATP permeability. It does, however, provide a sound structural basis for a Cl^--selective channel, as it is observed when the channel is activated by voltage or caspase cleavage (Ma et al., 2012; Romanov et al., 2012; Chiu et al., 2014; Wang and Dahl, 2018; Michalski et al., 2020). The external restriction has a width to accommodate Cl^- to pass through the channel when it is unobstructed by other channel components. Furthermore, the presence of positively charged amino acids could be the basis for anion selectivity. Indeed, mutations of R75 support this notion. The anion selectivity was preserved if R75 was changed to K, while a change to A not only diminished the Cl^- selectivity but also promoted cation permeability (Michalski et al., 2020). Because overlay of the structures of WT Panx1 and the truncated version mimicking the caspase-cleaved Panx1 did not reveal changes in the external constriction (Mou et al., 2020), it can be expected that both exhibit the same exclusion limits and Cl^- selectivity (Fig. 1).

Taken at face value, the presently available Panx1 channel structures do not support an ATP-release function of Panx1. Abundant functional data, on the other hand, are consistent with such a function. Therefore, one may consider that Panx1 exhibits an additional conformation not captured in the cryo-EM studies so far. How could a structure of the ATP-permeable Panx1 conformation be obtained? To boost the chance to observe the large-pore conformation of the Panx1 channel, it may be advantageous to activate Panx1 through ligand binding to G protein–coupled receptors, known to activate Panx1 in the process of secondary ATP release (Locovei et al., 2006b; Billaud et al., 2012; Murali et al., 2014; Dahl, 2018). For example, there is ample evidence that activation of Panx1 through $P2X_7$ and NMDA receptors involves the action of the Src gene product on Panx1, likely by tyrosine phosphorylation of the Panx1 protein itself (Weilinger et al., 2012; DeLalio et al., 2019; Lohman et al., 2019).

To test whether Panx1 phosphorylation per se is sufficient to drive the Panx1 channel to the open conformation, a Panx1 channel in an excised patch could be exposed to the active form of Src in the presence of ATP. If successful, the cryo-EM sample could be treated likewise to enhance the chance to capture the ATP-permeable conformation.

Other soluble potential activators of Panx1 include K^+ and Ca^{2+}. Although micromolar concentrations of Ca^{2+} were observed to activate large channels in inside-out membrane patches excised from oocytes expressing Panx1 (Locovei et al., 2006b), activation of Panx1 by Ca^{2+} was not observed in HEK cells (Ma et al., 2009). In contrast, secondary ATP release in carotid body type II cells was found to be attenuated by the Ca^{2+} chelator BAPTA (1,2-bis(*o*-aminophenoxy)ethane-N,N,N′,N′-tetraacetic acid; Murali et al., 2014), indicating Ca^{2+} involvement in Panx1 activation. Furthermore, it has been proposed that the activation of Panx1 by the mechanosensitive Piezo channels involves cytoplasmic $[Ca^{2+}]$ (Cinar et al., 2015; Wang et al., 2016; Diem et al., 2020). Although K^+ and Ca^{2+} failed to alter the cryo-EM structure (Ruan et al., 2020), it is not clear whether all possible iterations of the experimental approach have been exhausted.

Alternatively, the Panx1-$P2X_7$ complex is particularly interesting because these proteins interact physically and functionally (Pelegrin and Surprenant, 2006; Locovei et al., 2007; Iglesias et al., 2008; Silverman et al., 2009). Cryo-EM of the complex of Panx1 and P2X7 with and without ATP not only may allow the capture of the large pore conformation but may also yield clues about the gating mechanism. In both approaches, the ATP concentration has to be carefully chosen, since high concentrations of ATP were found to inhibit Panx1-mediated currents (Qiu and Dahl, 2009; Qiu et al., 2012).

Contribution of the C terminus to the pore structure

None of the cryo-EM structures published so far has resolved the C terminus. Only one paper shows an amorphous mass at the cytoplasmic entry to the channel (Ruan et al., 2020). It is noteworthy that all cryo-EM structures presently available were obtained with C terminus–tagged Panx1. It is conceivable that the C terminus was misfolded because of the tags and consequently escaped resolution. Resolution of the C terminus is important, since functional data strongly indicate a decisive role of the C terminus in channel function, in terms of both gating and permeability (Chekeni et al., 2010; Chiu et al., 2014; Jackson et al., 2014). In the voltage-activated and Cl^--selective channel, the terminal cysteine moiety is reactive to externally applied

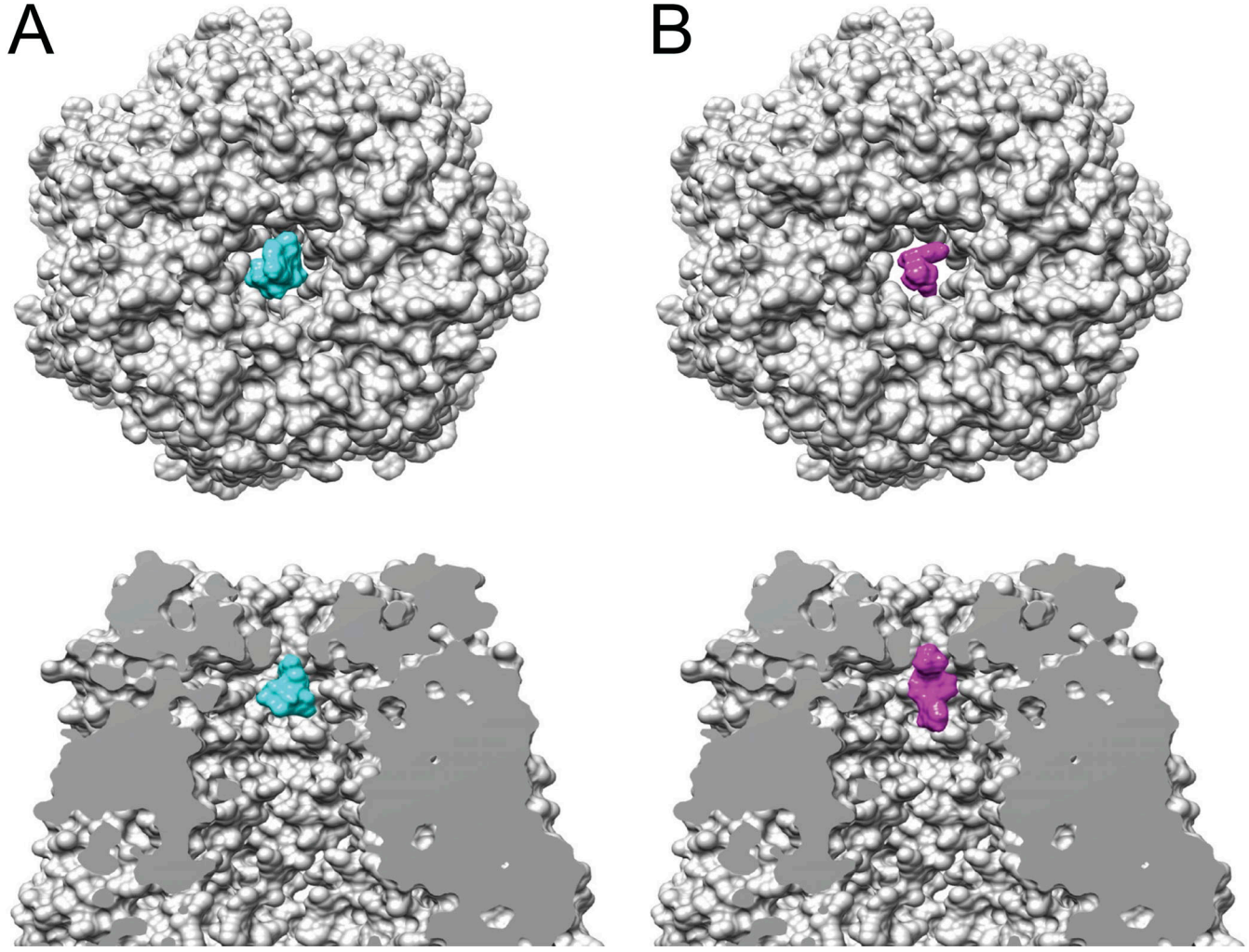

Figure 4. **Space-filling model of Panx1 without the C terminus.** Related to PDB accession no. 6wbg. **(A)** Top: Top view of the extracellular pore. The space-filling model of ATP (PubChem accession no. 5957, mol wt 507.2) is shown in cyan. Bottom: Side view of the extracellular pore showing the W 74 ring above the ATP. **(B)** Top: The same model as in A, top view of the extracellular pore. In magenta is the space-filling model of Yo-Pro-1 (PubChem accession no. 6913121, mol wt 375.5). Bottom: Side views of the extracellular pore with a model for Yo-Pro (magenta) placed at the level of the external constriction.

thiol reagents, as indicated by attenuation of Panx1-mediated membrane currents (Wang and Dahl, 2010). Furthermore, an analysis of pore-lining moieties by the substituted cysteine accessibility method showed that cysteine replacements of several amino acids in the C terminus exhibited reactivity to thiol reagents (Wang and Dahl, 2010), indicating that this terminus protrudes from the cytoplasmic site far into the channel permeation pathway. Further support for this conclusion comes from the observation that the endogenous C-terminal cysteine C426 interacted with Panx1F54C via a disulfide bond (Sandilos et al., 2012). The F54C position was identified as a pore lining moiety together with other positions in the first TM segment and the first extracellular loop of Panx1 in the substituted cysteine accessibility method analysis (Wang and Dahl, 2010). F54 is located in the proximity of I58 (Fig. 1 B), which is part of a second constriction (13 Å in diameter) of the permeation pathway (Deng et al., 2020). This observation suggests that the WT Panx1 cysteine C426 would be located a few angstroms from the extracellular surface in the voltage-activated channel.

Given that a large stretch of C-terminal amino acids fills the pore from the intracellular vestibule up to close to the extracellular restriction, one would expect that removal of the C terminus by caspase cleavage should affect the unitary conductance of the Panx1 channel to some extent. However, the WT Panx1 and truncated or caspase-cleaved Panx1 channels exhibit similar unitary conductances (Ma et al., 2012; Romanov et al., 2012; Chiu et al., 2014; Wang et al., 2014; Chiu et al., 2017)

Removal of the C terminus by caspase cleavage in apoptotic cells or genetically by placing a stop codon at the cleavage site renders the channel constitutively active, with sojourns to open and closed states (Chekeni et al., 2010; Chiu et al., 2014; Chiu et al., 2017). However, since nonapoptotic ATP release is reversible in most cells, cleavage cannot be an obligate step to transform the Cl^--selective and cation-impermeant conformation to the large-pore conformation, which allows the flux of ATP and is also cation permeant. Thus, for nonapoptotic ATP release, instead of being cleaved, the C terminus has to undergo a major rearrangement to move out of the permeation pathway for

adopting the ATP-permeable large-pore conformation. Indeed, in the large-pore conformation, the terminal cysteine was not further reactive to externally applied thiol reagents, while engineered cysteines at the external pore entry remained reactive (Wang et al., 2014). Energetically, the most favorable scenario would be a swinging out of the intact C terminus into a gap between TM helices created by a gating mechanism for the physiological, i.e., reversible activation of the large pore conformation.

An overlay of truncated and WT Panx1 cryo-EM structures did not reveal differences in the extracellular pore structure (Fig. 1; Mou et al., 2020). Thus, cleavage of the C terminus of Panx1 may not be sufficient to alter the pore conformation, which is consistent with identical selectivities of channels formed by WT and truncated Panx1. Consequently, the structure of the truncated Panx1 channel cannot account for ATP permeability of the full-length channel.

Ruan et al. (2020) suggested an intriguing hypothesis for the existence of different selectivities of the Panx1 channel. According to this hypothesis, the pathway for selective Cl^- flux involves a side tunnel, while the main pore is blocked by the C terminus residing in the intracellular vestibule. Movement or cleavage of the C terminus then would provide the ATP-permeable large-pore conformation. However, the functional data listed above, including thiol reaction of the terminal cysteine (Wang and Dahl, 2010) and cross-linking of it with an engineered cysteine in a position close to the external constriction (Sandilos et al., 2012), indicate that the C terminus extends deep into the channel pore and thus are not consistent with a role of a side tunnel. Furthermore, the reported restriction at the extracellular end of the pore still would exclude ATP molecules.

At present, the available information about the C terminus is restricted to functional data, since none of the published cryo-EM structures has this part of the protein resolved. The functional observations listed above suggest that the C terminus reaches from the intracellular site deep into the channel pore, probably occluding it in the closed state (Fig. 5 A). It can be hypothesized that at positive potential, the C terminus is rearranged (Fig. 5 B) so that the C-terminal cysteine moiety can react with extracellularly applied thiol reagents. The rearrangement of the C terminus allows mainly Cl^- to pass through the external restriction depicted in the cryo-EM structures, which imposes Cl^- selectivity. Alternatively, the C terminus is cleaved by caspase with the same consequences, plus the channel becoming constitutively active at negative and positive potentials (Fig. 5 C). Physiological stimuli, such as mechanical stress, directly or via Piezo (Cinar et al., 2015; Diem et al., 2020), initiate a gating mechanism, which widens the external constriction to accommodate the passage of ATP and render the channel nonselective for ions. In addition, the C terminus undergoes a conformational change, so that the terminal cysteine becomes inaccessible to thiol reagents (or a reaction does not affect membrane currents in this conformation). Extracellular K^+ can mimic the effect of the physiological stimuli (Fig. 5 D). Cleavage of the C terminus then solidifies the apoptotic fate of the cell (Fig. 5 E). Alternatively, the caspase-cleaved Panx1 channel can be "hyperactivated" to render the Cl^--selective conformation to the nonselective large-pore conformation (Fig. 5, C–E).

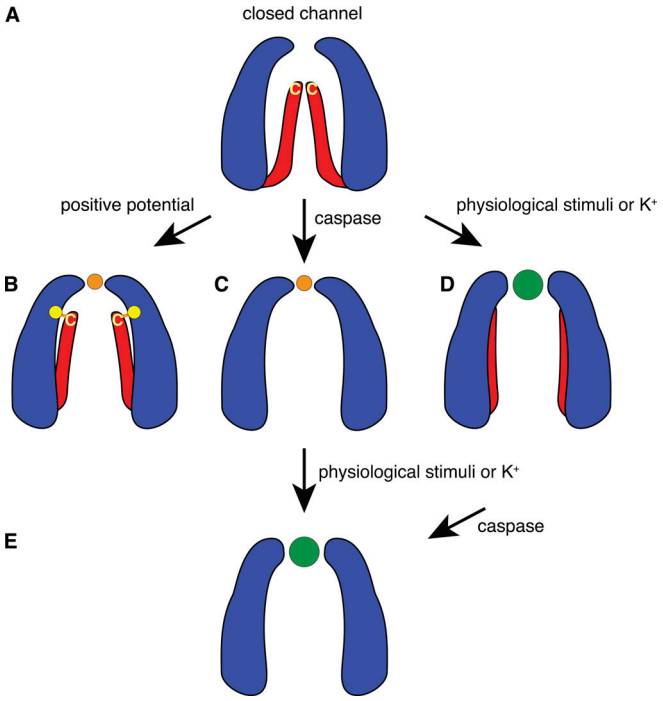

Figure 5. **Activation mechanisms of Panx1 channels. (A)** Based on the presently available structural and functional data, we hypothesize that the closed channel exhibits the external restriction of ∼9 Å and that the C termini reach deep into the pore, occluding it. **(B)** Depolarization dislocates the C termini, so that the channel pore diameter equals or exceeds that of the external restriction and exposes the terminal cysteine (yellow C) to thiol reagents. The yellow dot indicates the position of Panx1F54 which, when mutated to a cysteine, can be disulfide bonded with the terminal cysteine (Sandilos et al., 2012). In this configuration, the external restriction limits entry by size and selects for chloride (orange dot) over other ions. **(C)** Cleavage of Panx1 at position 378 removes the "pore gate," rendering the channel constitutively active. However, as indicated by the published cryo-EM data, caspase cleavage does not affect the external constriction, leaving a chloride-selective channel. **(D)** Various physiological stimuli initiate a gating mechanism at the external restriction, widening it to accept ATP (green dot) and other molecules in this size range. **(E)** This mechanism also may move charged amino acids within the external constriction, with the consequence that charge selectivity is attenuated. In the case of K^+ stimulation, the terminal cysteine is no further reactive to thiol reagents, while engineered cysteines at the external end of the pore still are. Whether this terminal cysteine concealment also applies to the physiological stimuli remains to be determined. Cleavage of the C terminus by caspase "super stimulates" the channel and irreversibly seals the apoptotic fate of the cell.

In theory, an alternative mechanism to switch the Cl^--selective channel to an ATP-permeable conformation would be a change of the oligomeric state of the channel. Such a mechanism may operate in CALHM 4 channels, for which cryo-EM data suggest the coexistence of decameric and undecameric channels, which exhibit different pore diameters (Drożdżyk et al., 2020). Furthermore, other large-pore channels such as gasdermin appear to have variable oligomeric states (Mulvihill et al., 2018). No experimental evidence for such a mechanism operating for Panx1 channels is presently in existence, though.

Problems to be solved

The cryo-EM structures of the Panx1 channel published in rapid succession have raised a number of crucial questions. While they

are consistent with the chloride-selective conformation of Panx1, they do not support an ATP-release function of this channel despite the abundance of evidence for such a role from functional data. The following points need to be addressed in future studies.

Although not likely, it is possible that the heptameric organization of the Panx1 channel could be a consequence of the procedures involved in cryo-EM. It would be desirable to have this oligomeric state verified by independent methods.

The published cryo-EM structures exhibit a restriction with a diameter of ∼9 Å, which would allow the passage of Cl^- but would be too small for the permeation of ATP. Considering, that innexin channels (innexons) are octamers and CALHM channels can be octamers, decamers, or undecamers (Choi et al., 2019; Drożdżyk et al., 2020; Syrjanen et al., 2020), one should not a priori rule out that the large-pore conformation is a higher-order oligomer.

For structural support of the ATP-release function of Panx1, a large-pore conformation is required with a pore dimension fitting the effective hydrated diameter of ATP of ∼12 Å (Sabirov and Okada, 2004) or a hydrodynamic diameter of ∼15.4 Å (Rostovtseva and Bezrukov, 1998). The structures published so far fall short of that.

Further support for the ATP-release function of Panx1 could come from cryo-EM structures of Panx1 in the presence of ATP. ATP molecules located in a properly sized pore would represent the strongest evidence for the ATP-release function of this protein. Furthermore, extracellular ATP triggers a negative feedback mechanism inhibiting the channel (Qiu and Dahl, 2009; Qiu et al., 2012). This process involves the critical extracellular loop amino acids R75 and W74. Thus, ATP may be found docked to the pore entry.

Because functional data strongly suggest that the C terminus of Panx1 can protrude deep into the channel pore, any functional conclusions from cryo-EM structures may be premature until the detailed C-terminal structure is resolved.

Because several receptors associate (at least functionally) with Panx1 to induce secondary ATP release, a cryo-EM structure of receptor-Panx1 complexes may not only reveal the type of physical interaction but may also enhance the chance of capturing the large-pore conformation by including the respective receptor ligands.

The puzzling observation that the forced hexameric channel has the same biophysical properties as the presumably heptameric WT channel needs a plausible explanation.

The channels formed by WT Panx1 and by caspase-cleaved or truncated Panx1 have been reported to have the same unitary conductances. Why does removal of a "pore plug" (the C terminus) not affect unitary conductance of the channel?

It is accepted that the voltage-activated Panx1 channel has a unitary conductance of 50–90 pS at positive potentials (Ma et al., 2012; Romanov et al., 2012; Wang et al., 2014; Chiu et al., 2018). However, what is the "unitary" conductance of the Panx1 channel in its large-pore conformation? Several laboratories have reported a ∼500-pS conductance for this channel conformation (Bao et al., 2004; Thompson et al., 2006; Kienitz et al., 2011; Orellana et al., 2011; Kurtenbach et al., 2013; Wang et al., 2014). Typically, in most recordings this large unitary conductance is a rare occurrence since the channel mainly dwells in one of the several subconductance states for extended periods of time. Thus, the term unitary can be misleading, and "maximal" conductance describes the situation better. However, a conductance of <100 pS at high positive membrane potentials and ∼15 pS at negative potentials has been proposed to be correlated with ATP release (Chiu et al., 2017). It is unclear, however, whether this lower conductance is actually a stable subconductance state or a record of the chloride-selective conformation. The latter is suggested by the similarity to the exclusively voltage-activated channel (Ma et al., 2012; Romanov et al., 2012; Wang et al., 2014). Reconstitution of the Panx1 protein into lipid bilayers yielded channel conductances of ∼1,000 pS (Mou et al., 2020). Whether this value is truly a single-channel conductance or whether the bilayer contained at least two active 500-pS channels remains to be determined.

In summary, the structural models from cryo-EM are consistent with each other and with electrophysiological recordings that describe a Panx1 channel that is selectively permeable to Cl^-. However, the models' small predicted pore sizes are insufficient to explain the considerable body of data showing that Panx1 is permeable to ATP and cations both physiologically and in apoptotic cells. Our previous experiments have suggested that Panx1 may work in more than one conformation, and this Viewpoint proposes ways to find a structural evidence for this hypothesis.

Acknowledgments

Crina M. Nimigean served as editor.

We thank Dr. Ken Muller for critically reading an early version of the manuscript.

This work was supported by a grant from the National Institutes of Health (R56HL136291 to G. Dahl and G. Perkins).

The authors declare no competing financial interests.

Author contributions: C. Mim, G. Perkins, and G. Dahl jointly conceived, wrote, and edited the manuscript.

References

Bao, L., S. Locovei, and G. Dahl. 2004. Pannexin membrane channels are mechanosensitive conduits for ATP. *FEBS Lett.* 572:65–68. https://doi.org/10.1016/j.febslet.2004.07.009

Billaud, M., A.W. Lohman, A.C. Straub, R. Looft-Wilson, S.R. Johnstone, C.A. Araj, A.K. Best, F.B. Chekeni, K.S. Ravichandran, S. Penuela, et al. 2011. Pannexin1 regulates α1-adrenergic receptor-mediated vasoconstriction. *Circ. Res.* 109:80–85. https://doi.org/10.1161/CIRCRESAHA.110.237594

Billaud, M., J.K. Sandilos, and B.E. Isakson. 2012. Pannexin 1 in the regulation of vascular tone. *Trends Cardiovasc. Med.* 22:68–72. https://doi.org/10.1016/j.tcm.2012.06.014

Boassa, D., C. Ambrosi, F. Qiu, G. Dahl, G. Gaietta, and G. Sosinsky. 2007. Pannexin1 channels contain a glycosylation site that targets the hexamer to the plasma membrane. *J. Biol. Chem.* 282:31733–31743. https://doi.org/10.1074/jbc.M702422200

Boassa, D., F. Qiu, G. Dahl, and G. Sosinsky. 2008. Trafficking dynamics of glycosylated pannexin 1 proteins. *Cell Commun. Adhes.* 15:119–132. https://doi.org/10.1080/15419060802013885

Boyd-Tressler, A., S. Penuela, D.W. Laird, and G.R. Dubyak. 2014. Chemotherapeutic drugs induce ATP release via caspase-gated pannexin-1 channels and a caspase/pannexin-1-independent mechanism. *J. Biol. Chem.* 289:27246–27263. https://doi.org/10.1074/jbc.M114.590240

Bruzzone, R., S.G. Hormuzdi, M.T. Barbe, A. Herb, and H. Monyer. 2003. Pannexins, a family of gap junction proteins expressed in brain. *Proc. Natl. Acad. Sci. USA.* 100:13644–13649. https://doi.org/10.1073/pnas.2233464100

Bunse, S., S. Locovei, M. Schmidt, F. Qiu, G. Zoidl, G. Dahl, and R. Dermietzel. 2009. The potassium channel subunit Kvbeta3 interacts with pannexin 1 and attenuates its sensitivity to changes in redox potentials. *FEBS J.* 276:6258–6270. https://doi.org/10.1111/j.1742-4658.2009.07334.x

Bunse, S., M. Schmidt, S. Hoffmann, K. Engelhardt, G. Zoidl, and R. Dermietzel. 2011. Single cysteines in the extracellular and transmembrane regions modulate pannexin 1 channel function. *J. Membr. Biol.* 244: 21–33. https://doi.org/10.1007/s00232-011-9393-3

Chekeni, F.B., M.R. Elliott, J.K. Sandilos, S.F. Walk, J.M. Kinchen, E.R. Lazarowski, A.J. Armstrong, S. Penuela, D.W. Laird, G.S. Salvesen, et al. 2010. Pannexin 1 channels mediate 'find-me' signal release and membrane permeability during apoptosis. *Nature.* 467:863–867. https://doi.org/10.1038/nature09413

Chiu, Y.H., X. Jin, C.B. Medina, S.A. Leonhardt, V. Kiessling, B.C. Bennett, S. Shu, L.K. Tamm, M. Yeager, K.S. Ravichandran, and D.A. Bayliss. 2017. A quantized mechanism for activation of pannexin channels. *Nat. Commun.* 8:14324. https://doi.org/10.1038/ncomms14324

Chiu, Y.H., K.S. Ravichandran, and D.A. Bayliss. 2014. Intrinsic properties and regulation of Pannexin 1 channel. *Channels (Austin).* 8:103–109. https://doi.org/10.4161/chan.27545

Chiu, Y.H., M.S. Schappe, B.N. Desai, and D.A. Bayliss. 2018. Revisiting multimodal activation and channel properties of Pannexin 1. *J. Gen. Physiol.* 150:19–39. https://doi.org/10.1085/jgp.201711888

Choi, W., N. Clemente, W. Sun, J. Du, and W. Lü. 2019. The structures and gating mechanism of human calcium homeostasis modulator 2. *Nature.* 576:163–167. https://doi.org/10.1038/s41586-019-1781-3

Cinar, E., S. Zhou, J. DeCourcey, Y. Wang, R.E. Waugh, and J. Wan. 2015. Piezo1 regulates mechanotransductive release of ATP from human RBCs. *Proc. Natl. Acad. Sci. USA.* 112:11783–11788. https://doi.org/10.1073/pnas.1507309112

Colombini, M. 2012. VDAC structure, selectivity, and dynamics. *Biochim. Biophys. Acta.* 1818:1457–1465. https://doi.org/10.1016/j.bbamem.2011.12.026

Dahl, G. 2015. ATP release through pannexon channels. *Philos. Trans. R. Soc. Lond. B Biol. Sci.* 370:20140191. https://doi.org/10.1098/rstb.2014.0191

Dahl, G. 2018. The Pannexin1 membrane channel: distinct conformations and functions. *FEBS Lett.* 592:3201–3209. https://doi.org/10.1002/1873-3468.13115

Dahl, G., and S. Locovei. 2006. Pannexin: to gap or not to gap, is that a question? *IUBMB Life.* 58:409–419. https://doi.org/10.1080/15216540600794526

Dahl, G., and K.J. Muller. 2014. Innexin and pannexin channels and their signaling. *FEBS Lett.* 588:1396–1402. https://doi.org/10.1016/j.febslet.2014.03.007

de Vasconcelos, N.M., N. Van Opdenbosch, H. Van Gorp, E. Parthoens, and M. Lamkanfi. 2019. Single-cell analysis of pyroptosis dynamics reveals conserved GSDMD-mediated subcellular events that precede plasma membrane rupture. *Cell Death Differ.* 26:146–161. https://doi.org/10.1038/s41418-018-0106-7

DeLalio, L.J., M. Billaud, C.A. Ruddiman, S.R. Johnstone, J.T. Butcher, A.G. Wolpe, X. Jin, T.C.S. Keller IV, A.S. Keller, T. Rivière, et al. 2019. Constitutive SRC-mediated phosphorylation of pannexin 1 at tyrosine 198 occurs at the plasma membrane. *J. Biol. Chem.* 294:6940–6956. https://doi.org/10.1074/jbc.RA118.006982

Deneka, D., M. Sawicka, A.K.M. Lam, C. Paulino, and R. Dutzler. 2018. Structure of a volume-regulated anion channel of the LRRC8 family. *Nature.* 558:254–259. https://doi.org/10.1038/s41586-018-0134-y

Deng, Z., Z. He, G. Maksaev, R.M. Bitter, M. Rau, J.A.J. Fitzpatrick, and P. Yuan. 2020. Cryo-EM structures of the ATP release channel pannexin 1. *Nat. Struct. Mol. Biol.* 27:373–381. https://doi.org/10.1038/s41594-020-0401-0

Diem, K., M. Fauler, G. Fois, A. Hellmann, N. Winokurow, S. Schumacher, C. Kranz, and M. Frick. 2020. Mechanical stretch activates piezo1 in caveolae of alveolar type I cells to trigger ATP release and paracrine stimulation of surfactant secretion from alveolar type II cells. *FASEB J.* 34:12785–12804. https://doi.org/10.1096/fj.202000613RRR

Drożdżyk, K., M. Sawicka, M.I. Bahamonde-Santos, Z. Jonas, D. Deneka, C. Albrecht, and R. Dutzler. 2020. Cryo-EM structures and functional properties of CALHM channels of the human placenta. *eLife.* 9:e55853. https://doi.org/10.7554/eLife.55853

Duan, Y., C.L. Sahley, and K.J. Muller. 2009. ATP and NO dually control migration of microglia to nerve lesions. *Dev. Neurobiol.* 69:60–72. https://doi.org/10.1002/dneu.20689

Epp, A.L., S.N. Ebert, J.C. Sanchez-Arias, L.E. Wicki-Stordeur, A.K.J. Boyce, and L.A. Swayne. 2019. A novel motif in the proximal C-terminus of Pannexin 1 regulates cell surface localization. *Sci. Rep.* 9:9721. https://doi.org/10.1038/s41598-019-46144-5

Flores, J.A., B.G. Haddad, K.A. Dolan, J.B. Myers, C.C. Yoshioka, J. Copperman, D.M. Zuckerman, and S.L. Reichow. 2020. Connexin-46/50 in a dynamic lipid environment resolved by CryoEM at 1.9 Å. *Nat. Commun.* 11: 4331. https://doi.org/10.1038/s41467-020-18120-5

Forsyth, A.M., J. Wan, P.D. Owrutsky, M. Abkarian, and H.A. Stone. 2011. Multiscale approach to link red blood cell dynamics, shear viscosity, and ATP release. *Proc. Natl. Acad. Sci. USA.* 108:10986–10991. https://doi.org/10.1073/pnas.1101315108

Gidö, G., T. Kristián, and B.K. Siesjö. 1997. Extracellular potassium in a neocortical core area after transient focal ischemia. *Stroke.* 28:206–210. https://doi.org/10.1161/01.STR.28.1.206

Gründken, C., J. Hanske, S. Wengel, W. Reuter, A. Abdulazim, V.I. Shestopalov, R. Dermietzel, G. Zoidl, and N. Prochnow. 2011. Unified patch clamp protocol for the characterization of Pannexin 1 channels in isolated cells and acute brain slices. *J. Neurosci. Methods.* 199:15–25. https://doi.org/10.1016/j.jneumeth.2011.04.016

Hanner, F., L. Lam, M.T. Nguyen, A. Yu, and J. Peti-Peterdi. 2012. Intrarenal localization of the plasma membrane ATP channel pannexin1. *Am. J. Physiol. Renal Physiol.* 303:F1454–F1459. https://doi.org/10.1152/ajprenal.00206.2011

Hansen, D.B., Z.-C. Ye, K. Calloe, T.H. Braunstein, J.P. Hofgaard, B.R. Ransom, M.S. Nielsen, and N. MacAulay. 2014. Activation, permeability, and inhibition of astrocytic and neuronal large pore (hemi)channels. *J Biol Chem.* 289:26058–26073. https://doi.org/10.1074/jbc.M114.582155

Harris, A L. 2001. Emerging issues of connexin channels: biophysics fills the gap. *Q Rev Biophys.* 34:325–472. https://doi.org/10.1017/s0033583501003705

Heinrich, A., R.D. Andó, G. Túri, B. Rózsa, and B. Sperlágh. 2012. K+ depolarization evokes ATP, adenosine and glutamate release from glia in rat hippocampus: a microelectrode biosensor study. *Br. J. Pharmacol.* 167: 1003–1020. https://doi.org/10.1111/j.1476-5381.2012.01932.x

Huang, Y., J.B. Grinspan, C.K. Abrams, and S.S. Scherer. 2007. Pannexin1 is expressed by neurons and glia but does not form functional gap junctions. *Glia.* 55:46–56. https://doi.org/10.1002/glia.20435

Iglesias, R., G. Dahl, F. Qiu, D.C. Spray, and E. Scemes. 2009a. Pannexin 1: the molecular substrate of astrocyte "hemichannels". *J. Neurosci.* 29: 7092–7097. https://doi.org/10.1523/JNEUROSCI.6062-08.2009

Iglesias, R., S. Locovei, A. Roque, A.P. Alberto, G. Dahl, D.C. Spray, and E. Scemes. 2008. P2X7 receptor-Pannexin1 complex: pharmacology and signaling. *Am. J. Physiol. Cell Physiol.* 295:C752–C760. https://doi.org/10.1152/ajpcell.00228.2008

Iglesias, R., D.C. Spray, and E. Scemes. 2009b. Mefloquine blockade of Pannexin1 currents: resolution of a conflict. *Cell Commun. Adhes.* 16:131–137. https://doi.org/10.3109/15419061003642618

Imamura, H., S. Sakamoto, T. Yoshida, Y. Matsui, S. Penuela, D.W. Laird, S. Mizukami, K. Kikuchi, and A. Kakizuka. 2020. Single-cell dynamics of pannexin-1-facilitated programmed ATP loss during apoptosis. *eLife.* 9: e61960. https://doi.org/10.7554/eLife.61960

Jackson, D.G., J. Wang, R.W. Keane, E. Scemes, and G. Dahl. 2014. ATP and potassium ions: a deadly combination for astrocytes. *Sci. Rep.* 4:4576. https://doi.org/10.1038/srep04576

Jin, Q., B. Zhang, X. Zheng, N. Li, L. Xu, Y. Xie, F. Song, E.A. Bhat, Y. Chen, N. Gao, et al. 2020. Cryo-EM structures of human pannexin 1 channel. *Cell Res.* 30:449–451. https://doi.org/10.1038/s41422-020-0310-0

Johnson, R.G., H.C. Le, K. Evenson, S.W. Loberg, T.M. Myslajek, A. Prabhu, A.M. Manley, C. O'Shea, H. Grunenwald, M. Haddican, et al. 2016. Connexin Hemichannels: Methods for Dye Uptake and Leakage. *J. Membr. Biol.* 249:713–741. https://doi.org/10.1007/s00232-016-9925-y

Kashio, M., G. Wei-Qi, Y. Ohsaki, M.A. Kido, and A. Taruno. 2019. CALHM1/CALHM3 channel is intrinsically sorted to the basolateral membrane of epithelial cells including taste cells. *Sci. Rep.* 9:2681. https://doi.org/10.1038/s41598-019-39593-5

Kasuya, G., T. Nakane, T. Yokoyama, Y. Jia, M. Inoue, K. Watanabe, R. Nakamura, T. Nishizawa, T. Kusakizako, A. Tsutsumi, et al. 2018. Cryo-EM structures of the human volume-regulated anion channel LRRC8. *Nat. Struct. Mol. Biol.* 25:797–804. https://doi.org/10.1038/s41594-018-0109-6

Kefauver, J.M., K. Saotome, A.E. Dubin, J. Pallesen, C.A. Cottrell, S.M. Cahalan, Z. Qiu, G. Hong, C.S. Crowley, T. Whitwam, et al. 2018. Structure of the human volume regulated anion channel. *eLife.* 7:e38461. https://doi.org/10.7554/eLife.38461

Kienitz, M.C., K. Bender, R. Dermietzel, L. Pott, and G. Zoidl. 2011. Pannexin 1 constitutes the large conductance cation channel of cardiac myocytes. *J. Biol. Chem.* 286:290–298. https://doi.org/10.1074/jbc.M110.163477

Kurtenbach, S., N. Prochnow, S. Kurtenbach, J. Klooster, C. Zoidl, R. Dermietzel, M. Kamermans, and G. Zoidl. 2013. Pannexin1 channel proteins in the zebrafish retina have shared and unique properties. *PLoS One.* 8: e77722. https://doi.org/10.1371/journal.pone.0077722

Lee, H.J., H. Jeong, J. Hyun, B. Ryu, K. Park, H.H. Lim, J. Yoo, and J.S. Woo. 2020. Cryo-EM structure of human Cx31.3/GJC3 connexin hemichannel. *Sci. Adv.* 6:eaba4996. https://doi.org/10.1126/sciadv.aba4996

Li, G., Q. Zhang, J. Hong, J.K. Ritter, and P.L. Li. 2018. Inhibition of pannexin-1 channel activity by adiponectin in podocytes: Role of acid ceramidase activation. *Biochim. Biophys. Acta Mol. Cell Biol. Lipids.* 1863:1246–1256. https://doi.org/10.1016/j.bbalip.2018.07.016

Locovei, S., L. Bao, and G. Dahl. 2006a. Pannexin 1 in erythrocytes: function without a gap. *Proc. Natl. Acad. Sci. USA.* 103:7655–7659. https://doi.org/10.1073/pnas.0601037103

Locovei, S., E. Scemes, F. Qiu, D.C. Spray, and G. Dahl. 2007. Pannexin1 is part of the pore forming unit of the P2X(7) receptor death complex. *FEBS Lett.* 581:483–488. https://doi.org/10.1016/j.febslet.2006.12.056

Locovei, S., J. Wang, and G. Dahl. 2006b. Activation of pannexin 1 channels by ATP through P2Y receptors and by cytoplasmic calcium. *FEBS Lett.* 580: 239–244. https://doi.org/10.1016/j.febslet.2005.12.004

Lohman, A.W., N.L. Weilinger, S.M. Santos, J. Bialecki, A.C. Werner, C.L. Anderson, and R.J. Thompson. 2019. Regulation of pannexin channels in the central nervous system by Src family kinases. *Neurosci. Lett.* 695: 65–70. https://doi.org/10.1016/j.neulet.2017.09.019

Ma, W., V. Compan, W. Zheng, E. Martin, R.A. North, A. Verkhratsky, and A. Surprenant. 2012. Pannexin 1 forms an anion-selective channel. *Pflugers Arch.* 463:585–592. https://doi.org/10.1007/s00424-012-1077-z

Ma, W., H. Hui, P. Pelegrin, and A. Surprenant. 2009. Pharmacological characterization of pannexin-1 currents expressed in mammalian cells. *J. Pharmacol. Exp. Ther.* 328:409–418. https://doi.org/10.1124/jpet.108.146365

Ma, Z., J.E. Tanis, A. Taruno, and J.K. Foskett. 2016. Calcium homeostasis modulator (CALHM) ion channels. *Pflugers Arch.* 468:395–403. https://doi.org/10.1007/s00424-015-1757-6

MacVicar, B.A., and R.J. Thompson. 2010. Non-junction functions of pannexin-1 channels. *Trends Neurosci.* 33:93–102. https://doi.org/10.1016/j.tins.2009.11.007

Maeda, S., S. Nakagawa, M. Suga, E. Yamashita, A. Oshima, Y. Fujiyoshi, and T. Tsukihara. 2009. Structure of the connexin 26 gap junction channel at 3.5 A resolution. *Nature.* 458:597–602. https://doi.org/10.1038/nature07869

Medina, C.B., P. Mehrotra, S. Arandjelovic, J.S.A. Perry, Y. Guo, S. Morioka, B. Barron, S.F. Walk, B. Ghesquière, A.S. Krupnick, et al. 2020. Metabolites released from apoptotic cells act as tissue messengers. *Nature.* 580: 130–135. https://doi.org/10.1038/s41586-020-2121-3

Michalski, K., and T. Kawate. 2016. Carbenoxolone inhibits Pannexin1 channels through interactions in the first extracellular loop. *J. Gen. Physiol.* 147:165–174. https://doi.org/10.1085/jgp.201511505

Michalski, K., E. Henze, P. Nguyen, P. Lynch, and T. Kawate. 2018. The weak voltage dependence of pannexin 1 channels can be tuned by N-terminal modifications. *J. Gen. Physiol.* 150:1758–1768. https://doi.org/10.1085/jgp.201711804

Michalski, K., J.L. Syrjanen, E. Henze, J. Kumpf, H. Furukawa, and T. Kawate. 2020. The Cryo-EM structure of pannexin 1 reveals unique motifs for ion selection and inhibition. *eLife.* 9:e54670. https://doi.org/10.7554/eLife.54670

Mou, L., M. Ke, M. Song, Y. Shan, Q. Xiao, Q. Liu, J. Li, K. Sun, L. Pu, L. Guo, et al. 2020. Structural basis for gating mechanism of Pannexin 1 channel. *Cell Res.* 30:452–454. https://doi.org/10.1038/s41422-020-0313-x

Mulvihill, E., L. Sborgi, S.A. Mari, M. Pfreundschuh, S. Hiller, and D.J. Müller. 2018. Mechanism of membrane pore formation by human gasdermin-D. *EMBO J.* 37:e98321. https://doi.org/10.15252/embj.201798321

Murali, S., M. Zhang, and C.A. Nurse. 2014. Angiotensin II mobilizes intracellular calcium and activates pannexin-1 channels in rat carotid body type II cells via AT1 receptors. *J. Physiol.* 592:4747–4762. https://doi.org/10.1113/jphysiol.2014.279299

Myers, J.B., B.G. Haddad, S.E. O'Neill, D.S. Chorev, C.C. Yoshioka, C.V. Robinson, D.M. Zuckerman, and S.L. Reichow. 2018. Structure of native lens connexin 46/50 intercellular channels by cryo-EM. *Nature.* 564: 372–377. https://doi.org/10.1038/s41586-018-0786-7

Narahari, A.K., A.J. Kreutzberger, P.S. Gaete, Y.H. Chiu, S.A. Leonhardt, C.B. Medina, X. Jin, P.W. Oleniacz, V. Kiessling, P.Q. Barrett, et al. 2021. ATP and large signaling metabolites flux through caspase-activated Pannexin 1 channels. *eLife.* 10:e64787. https://doi.org/10.7554/eLife.64787

Nielsen, B.S., T.L. Toft-Bertelsen, S.D. Lolansen, C.L. Anderson, M.S. Nielsen, R.J. Thompson, and N. MacAulay. 2020. Pannexin 1 activation and inhibition is permeant-selective. *J. Physiol.* 598:361–379. https://doi.org/10.1113/JP278759

Nielsen, M.S., L.N. Axelsen, P.L. Sorgen, V. Verma, M. Delmar, and N.H. Holstein-Rathlou. 2012. Gap junctions. *Compr. Physiol.* 2:1981–2035.

Nomura, T., A. Taruno, M. Shiraishi, T. Nakahari, T. Inui, M. Sokabe, D.C. Eaton, and Y. Marunaka. 2017. Current-direction/amplitude-dependent single channel gating kinetics of mouse pannexin 1 channel: a new concept for gating kinetics. *Sci. Rep.* 7:10512. https://doi.org/10.1038/s41598-017-10921-x

Orellana, J.A., K.F. Shoji, V. Abudara, P. Ezan, E. Amigou, P.J. Sáez, J.X. Jiang, C.C. Naus, J.C. Sáez, and C. Giaume. 2011. Amyloid β-induced death in neurons involves glial and neuronal hemichannels. *J. Neurosci.* 31: 4962–4977. https://doi.org/10.1523/JNEUROSCI.6417-10.2011

Osei-Owusu, J., J. Yang, M.D.C. Vitery, and Z. Qiu. 2018. Molecular Biology and Physiology of Volume-Regulated Anion Channel (VRAC). *Curr. Top. Membr.* 81:177–203. https://doi.org/10.1016/bs.ctm.2018.07.005

Oshima, A., K. Tani, and Y. Fujiyoshi. 2016. Atomic structure of the innexin-6 gap junction channel determined by cryo-EM. *Nat. Commun.* 7:13681. https://doi.org/10.1038/ncomms13681

Panchin, Y., I. Kelmanson, M. Matz, K. Lukyanov, N. Usman, and S. Lukyanov. 2000. A ubiquitous family of putative gap junction molecules. *Curr. Biol.* 10:R473–R474. https://doi.org/10.1016/S0960-9822(00)00576-5

Pelegrin, P., and A. Surprenant. 2006. Pannexin-1 mediates large pore formation and interleukin-1beta release by the ATP-gated P2X7 receptor. *EMBO J.* 25:5071–5082. https://doi.org/10.1038/sj.emboj.7601378

Penuela, S., R. Bhalla, X.Q. Gong, K.N. Cowan, S.J. Celetti, B.J. Cowan, D. Bai, Q. Shao, and D.W. Laird. 2007. Pannexin 1 and pannexin 3 are glycoproteins that exhibit many distinct characteristics from the connexin family of gap junction proteins. *J. Cell Sci.* 120:3772–3783. https://doi.org/10.1242/jcs.009514

Penuela, S., R. Gehi, and D.W. Laird. 2013. The biochemistry and function of pannexin channels. *Biochim. Biophys. Acta.* 1828:15–22. https://doi.org/10.1016/j.bbamem.2012.01.017

Prochnow, N., S. Hoffmann, R. Vroman, J. Klooster, S. Bunse, M. Kamermans, R. Dermietzel, and G. Zoidl. 2009. Pannexin1 in the outer retina of the zebrafish, Danio rerio. *Neuroscience.* 162:1039–1054. https://doi.org/10.1016/j.neuroscience.2009.04.064

Qiu, F., and G. Dahl. 2009. A permeant regulating its permeation pore: inhibition of pannexin 1 channels by ATP. *Am. J. Physiol. Cell Physiol.* 296: C250–C255. https://doi.org/10.1152/ajpcell.00433.2008

Qiu, F., J. Wang, D.C. Spray, E. Scemes, and G. Dahl. 2011. Two non-vesicular ATP release pathways in the mouse erythrocyte membrane. *FEBS Lett.* 585:3430–3435. https://doi.org/10.1016/j.febslet.2011.09.033

Qiu, F., J. Wang, and G. Dahl. 2012. Alanine substitution scanning of pannexin1 reveals amino acid residues mediating ATP sensitivity. *Purinergic Signal.* 8:81–90. https://doi.org/10.1007/s11302-011-9263-6

Qu, R., L. Dong, J. Zhang, X. Yu, L. Wang, and S. Zhu. 2020. Cryo-EM structure of human heptameric Pannexin 1 channel. *Cell Res.* 30: 446–448. https://doi.org/10.1038/s41422-020-0298-5

Qu, Y., S. Misaghi, K. Newton, L.L. Gilmour, S. Louie, J.E. Cupp, G.R. Dubyak, D. Hackos, and V.M. Dixit. 2011. Pannexin-1 is required for ATP release during apoptosis but not for inflammasome activation. *J. Immunol.* 186: 6553–6561. https://doi.org/10.4049/jimmunol.1100478

Ransford, G.A., N. Fregien, F. Qiu, G. Dahl, G.E. Conner, and M. Salathe. 2009. Pannexin 1 contributes to ATP release in airway epithelia. *Am. J. Respir. Cell Mol. Biol.* 41:525–534. https://doi.org/10.1165/rcmb.2008-0367OC

Romanov, R.A., M.F. Bystrova, O.A. Rogachevskaya, V.B. Sadovnikov, V.I. Shestopalov, and S.S. Kolesnikov. 2012. The ATP permeability of pannexin 1 channels in a heterologous system and in mammalian taste cells is dispensable. *J. Cell Sci.* 125:5514–5523. https://doi.org/10.1242/jcs.111062

Rostovtseva, T.K., and S.M. Bezrukov. 1998. ATP transport through a single mitochondrial channel, VDAC, studied by current fluctuation analysis. *Biophys. J.* 74:2365–2373. https://doi.org/10.1016/S0006-3495(98)77945-7

Ruan, Z., I.J. Orozco, J. Du, and W. Lü. 2020. Structures of human pannexin 1 reveal ion pathways and mechanism of gating. *Nature.* 584:646–651. https://doi.org/10.1038/s41586-020-2357-y

Sabirov, R.Z., and Y. Okada. 2004. Wide nanoscopic pore of maxi-anion channel suits its function as an ATP-conductive pathway. *Biophys. J.* 87:1672–1685. https://doi.org/10.1529/biophysj.104.043174

Samuels, S.E., J.B. Lipitz, G. Dahl, and K.J. Muller. 2010. Neuroglial ATP release through innexin channels controls microglial cell movement to a

nerve injury. *J. Gen. Physiol.* 136:425–442. https://doi.org/10.1085/jgp.201010476

Samuels, S.E., J.B. Lipitz, J. Wang, G. Dahl, and K.J. Muller. 2013. Arachidonic acid closes innexin/pannexin channels and thereby inhibits microglia cell movement to a nerve injury. *Dev. Neurobiol.* 73:621–631. https://doi.org/10.1002/dneu.22088

Sandilos, J.K., Y.H. Chiu, F.B. Chekeni, A.J. Armstrong, S.F. Walk, K.S. Ravichandran, and D.A. Bayliss. 2012. Pannexin 1, an ATP release channel, is activated by caspase cleavage of its pore-associated C-terminal autoinhibitory region. *J. Biol. Chem.* 287:11303–11311. https://doi.org/10.1074/jbc.M111.323378

Santiago, M.F., J. Veliskova, N.K. Patel, S.E. Lutz, D. Caille, A. Charollais, P. Meda, and E. Scemes. 2011. Targeting pannexin1 improves seizure outcome. *PLoS One.* 6:e25178. https://doi.org/10.1371/journal.pone.0025178

Scemes, E., S.O. Suadicani, G. Dahl, and D.C. Spray. 2007. Connexin and pannexin mediated cell-cell communication. *Neuron Glia Biol.* 3:199–208. https://doi.org/10.1017/S1740925X08000069

Shum, M.G., Q. Shao, P. Lajoie, and D.W. Laird. 2019. Destination and consequences of Panx1 and mutant expression in polarized MDCK cells. *Exp. Cell Res.* 381:235–247. https://doi.org/10.1016/j.yexcr.2019.05.016

Sick, T.J., Z.C. Feng, and M. Rosenthal. 1998. Spatial stability of extracellular potassium ion and blood flow distribution in rat cerebral cortex after permanent middle cerebral artery occlusion. *J. Cereb. Blood Flow Metab.* 18:1114–1120. https://doi.org/10.1097/00004647-199810000-00008

Siebert, A.P., Z. Ma, J.D. Grevet, A. Demuro, I. Parker, and J.K. Foskett. 2013. Structural and functional similarities of calcium homeostasis modulator 1 (CALHM1) ion channel with connexins, pannexins, and innexins. *J. Biol. Chem.* 288:6140–6153. https://doi.org/10.1074/jbc.M112.409789

Silverman, W.R., J.P. de Rivero Vaccari, S. Locovei, F. Qiu, S.K. Carlsson, E. Scemes, R.W. Keane, and G. Dahl. 2009. The pannexin 1 channel activates the inflammasome in neurons and astrocytes. *J. Biol. Chem.* 284:18143–18151. https://doi.org/10.1074/jbc.M109.004804

Somjen, G.G. 1979. Extracellular potassium in the mammalian central nervous system. *Annu. Rev. Physiol.* 41:159–177. https://doi.org/10.1146/annurev.ph.41.030179.001111

Sosinsky, G.E., D. Boassa, R. Dermietzel, H.S. Duffy, D.W. Laird, B. MacVicar, C.C. Naus, S. Penuela, E. Scemes, D.C. Spray, et al. 2011. Pannexin channels are not gap junction hemichannels. *Channels (Austin).* 5:193–197. https://doi.org/10.4161/chan.5.3.15765

Sridharan, M., S.P. Adderley, E.A. Bowles, T.M. Egan, A.H. Stephenson, M.L. Ellsworth, and R.S. Sprague. 2010. Pannexin 1 is the conduit for low oxygen tension-induced ATP release from human erythrocytes. *Am. J. Physiol. Heart Circ. Physiol.* 299:H1146–H1152. https://doi.org/10.1152/ajpheart.00301.2010

Srinivas, M., D.P. Calderon, J. Kronengold, and V.K. Verselis. 2006. Regulation of connexin hemichannels by monovalent cations. *J. Gen. Physiol.* 127:67–75. https://doi.org/10.1085/jgp.200509397

Suadicani, S.O., R. Iglesias, J. Wang, G. Dahl, D.C. Spray, and E. Scemes. 2012. ATP signaling is deficient in cultured Pannexin1-null mouse astrocytes. *Glia.* 60:1106–1116. https://doi.org/10.1002/glia.22338

Syrjanen, J.L., K. Michalski, T.H. Chou, T. Grant, S. Rao, N. Simorowski, S.J. Tucker, N. Grigorieff, and H. Furukawa. 2020. Structure and assembly of calcium homeostasis modulator proteins. *Nat. Struct. Mol. Biol.* 27:150–159. https://doi.org/10.1038/s41594-019-0369-9

Taruno, A., V. Vingtdeux, M. Ohmoto, Z. Ma, G. Dvoryanchikov, A. Li, L. Adrien, H. Zhao, S. Leung, M. Abernethy, et al. 2013. CALHM1 ion channel mediates purinergic neurotransmission of sweet, bitter and umami tastes. *Nature.* 495:223–226. https://doi.org/10.1038/nature11906

Thompson, R.J., M.F. Jackson, M.E. Olah, R.L. Rungta, D.J. Hines, M.A. Beazely, J.F. MacDonald, and B.A. MacVicar. 2008. Activation of pannexin-1 hemichannels augments aberrant bursting in the hippocampus. *Science.* 322:1555–1559. https://doi.org/10.1126/science.1165209

Thompson, R.J., N. Zhou, and B.A. MacVicar. 2006. Ischemia opens neuronal gap junction hemichannels. *Science.* 312:924–927. https://doi.org/10.1126/science.1126241

Wang, J., and G. Dahl. 2010. SCAM analysis of Panx1 suggests a peculiar pore structure. *J. Gen. Physiol.* 136:515–527. https://doi.org/10.1085/jgp.201010440

Wang, J., and G. Dahl. 2018. Pannexin1: a multifunction and multiconductance and/or permeability membrane channel. *Am. J. Physiol. Cell Physiol.* 315:C290–C299. https://doi.org/10.1152/ajpcell.00302.2017

Wang, J., C. Ambrosi, F. Qiu, D.G. Jackson, G. Sosinsky, and G. Dahl. 2014. The membrane protein Pannexin1 forms two open-channel conformations depending on the mode of activation. *Sci. Signal.* 7:ra69. https://doi.org/10.1126/scisignal.2005431

Wang, J., D.G. Jackson, and G. Dahl. 2013. The food dye FD&C Blue No. 1 is a selective inhibitor of the ATP release channel Panx1. *J. Gen. Physiol.* 141:649–656. https://doi.org/10.1085/jgp.201310966

Wang, J., D.G. Jackson, and G. Dahl. 2018. Cationic control of Panx1 channel function. *Am. J. Physiol. Cell Physiol.* 315:C279–C289. https://doi.org/10.1152/ajpcell.00303.2017

Wang, S., R. Chennupati, H. Kaur, A. Iring, N. Wettschureck, and S. Offermanns. 2016. Endothelial cation channel PIEZO1 controls blood pressure by mediating flow-induced ATP release. *J. Clin. Invest.* 126:4527–4536. https://doi.org/10.1172/JCI87343

Wei, Z.Y., H.L. Qu, Y.J. Dai, Q. Wang, Z.M. Ling, W.F. Su, Y.Y. Zhao, W.X. Shen, and G. Chen. 2021. Pannexin 1, a large-pore membrane channel, contributes to hypotonicity-induced ATP release in Schwann cells. *Neural Regen. Res.* 16:899–904. https://doi.org/10.4103/1673-5374.290911

Weilinger, N.L., P.L. Tang, and R.J. Thompson. 2012. Anoxia-induced NMDA receptor activation opens pannexin channels via Src family kinases. *J. Neurosci.* 32:12579–12588. https://doi.org/10.1523/JNEUROSCI.1267-12.2012

Zhan, H., C.S. Moore, B. Chen, X. Zhou, X.M. Ma, K. Ijichi, M.V. Bennett, X.J. Li, S.J. Crocker, and Z.W. Wang. 2012. Stomatin inhibits pannexin-1-mediated whole-cell currents by interacting with its carboxyl terminal. *PLoS One.* 7:e39489. https://doi.org/10.1371/journal.pone.0039489

Zhang, H., Z. Shen, B. Hogan, A.I. Barakat, and C. Misbah. 2018. ATP Release by Red Blood Cells under Flow: Model and Simulations. *Biophys. J.* 115:2218–2229. https://doi.org/10.1016/j.bpj.2018.09.033